# Hyperspectral Pansharpening: A Review



DATA FUSION IN REMOTE SENSING

IMAGE LICENSED BY INGRAM PUBLISHING
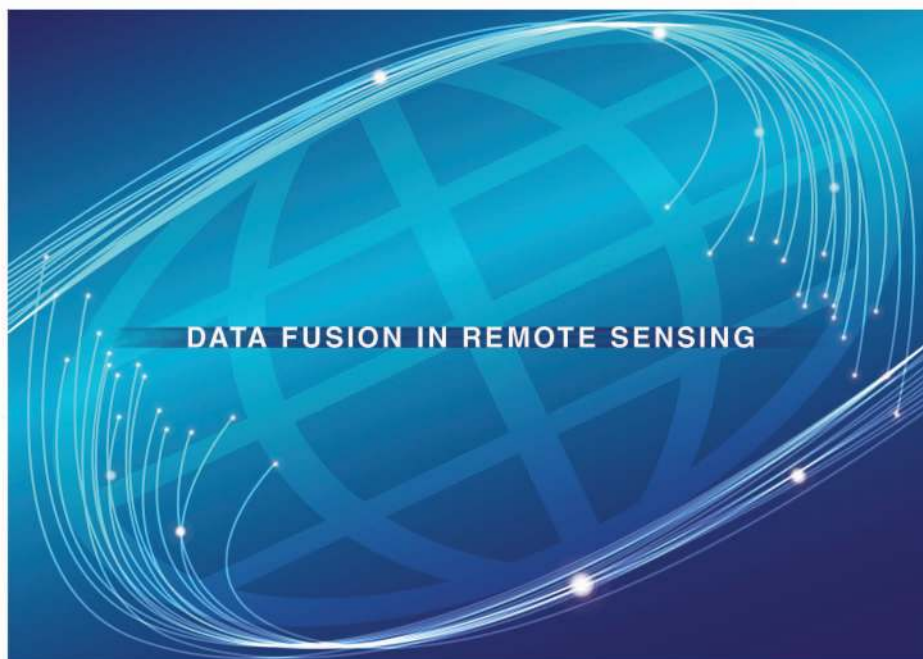
**LAETITIA LONCAN**
Gipsa-lab, Grenoble, France and ONERA, Toulouse, France
(e-mail: laetitia.loncan@onera.fr)

**LUÍS B. ALMEIDA AND JOSÉ M. BIOUCAS-DIAS**
Instituto de Telecomunicações, Instituto Superior Técnico,
Universidade de Lisboa
(e-mails: luis.almeida@lx.it.pt, bioucas@lx.it.pt)

**XAVIER BRIOTTET**
ONERA, Toulouse, France
(e-mail: Xavier.briottet@onera.fr)

**JOCELYN CHANUSSOT**
Gipsa-lab, Grenoble, France
(e-mail: Jocelyn.chanussot@gipsa-lab.grenoble-inp.fr)

**NICOLAS DOBIGEON**
University of Toulouse, IRIT/INP-ENSEEIHT
(e-mail: nicolas.dobigeon@enseeiht.fr)

**SOPHIE FABRE**
ONERA, Toulouse, France
(e-mail: Sophie.Fabre@onera.fr)

**WENZHI LIAO**
Ghent University, Ghent, Belgium
(e-mail: wliao@telin.ugent.be)

**GIORGIO A. LICCIARDI**
Gipsa-lab, Grenoble, France (e-mail: Giorgio-Antonino.
Licciardi@gipsa-lab.grenoble-inp.fr)

**MIGUEL SIMÕES**
Instituto de Telecomunicações, Instituto Superior Técnico,
Universidade de Lisboa and Gipsa-lab, Grenoble, France
(e-mail: miguel.simoes@lx.it.pt)

**JEAN-YVES TOURNERET**
University of Toulouse, IRIT/INP-ENSEEIHT
(e-mail: jean-yves.tourneret@enseeiht.fr)

**MIGUEL A. VEGANZONES**
Gipsa-lab, Grenoble, France
(e-mail: miguelangel.veganzones
@gipsa-lab.grenoble-inp.fr)

**GEMINE VIVONE**
North Atlantic Treaty Organization (NATO) Science
and Technology Organization (STO) Centre
for Maritime Research and Experimentation (CMRE)
(e-mail: gemine.vivone@cmre.nato.int)

**QI WEI**
University of Toulouse, IRIT/INP-ENSEEIHT
(e-mail: qi.wei@n7.fr)

**NAOTO YOKOYA**
University of Tokyo
(e-mail:yokoya@sal.rcast.u-tokyo.ac.jp)

*Abstract*—Pansharpening aims at fusing a panchromatic image with a multispectral one, to generate an image with the high spatial resolution of the former and the high spectral resolution of the latter. In the last decade, many algorithms have been presented in the literatures for pansharpening using multispectral data. With the increasing availability of hyperspectral systems, these methods are now being adapted to hyperspectral images. In this work, we compare new pansharpening techniques designed for hyperspectral data with some of the state-of-the-art methods for multispectral pansharpening, which have been adapted for hyperspectral data. Eleven methods from different classes (component substitution, multiresolution analysis, hybrid, Bayesian and matrix factorization) are analyzed. These methods are applied to three datasets and their effectiveness and robustness are evaluated with widely used performance indicators. In addition, all the pansharpening techniques considered in this paper have been implemented in a MATLAB toolbox that is made available to the community.

> **FUSING IMAGES WITH COMPLEMENTARY PROPERTIES, PANSHARPENING HELPS SYNTHETIZING A HYPERSPECTRAL IMAGE WITH A HIGH SPATIAL RESOLUTION.**

## I. INTRODUCTION

In the design of optical remote sensing systems, owing to the limited amount of incident energy, there are critical tradeoffs between the spatial resolution, the spectral resolution, and signal-to-noise ratio (SNR). For this reason, optical systems can provide data with a high spatial resolution but with a small number of spectral bands (for example, panchromatic data with decimetric spatial resolution or multispectral data with three to four bands and metric spatial resolution, like PLEIADES [1]) or with a high spectral resolution but with reduced spatial resolution (for example, hyperspectral data, subsequently referred to as HS data, with more than one hundred of bands and decametric spatial resolution like HYPXIM [2]). To enhance the spatial resolution of multispectral data, several methods have been proposed in the literature under the name of pansharpening, which is a form of superresolution. Fun-

damentally, these methods solve an inverse problem which consists of obtaining an enhanced image with both high spatial and high spectral resolutions from a panchromatic image and a multispectral image. The huge interest of the community on this topic is evidenced by the existence of sessions dedicated to this topic in the most important remote sensing and earth observation conferences as well as by the launch of public contests, of which the one sponsored by the data fusion committee of the IEEE Geoscience and Remote Sensing society [3] is an example.

A taxonomy of pansharpening methods can be found in the literature [4], [5], [6]. They can be broadly divided into four classes: component substitution (CS), multiresolution analysis (MRA), Bayesian, and variational. The CS approach relies on the substitution of a component (obtained, e.g., by a spectral transformation of the data) of the multispectral (subsequently denoted as MS) image by the panchromatic (subsequently denoted as PAN) image. The CS class contains algorithms such as intensity-hue-saturation (IHS) [7], [8], [9], principal component analysis (PCA) [10], [11], [12] and Gram-Schmidt (GS) spectral sharpening [13]. The MRA approach is based on the injection of spatial details, which are obtained through a multiscale decomposition of the PAN image into the MS data. The spatial details can be extracted according to several modalities of MRA: decimated wavelet transform (DWT) [14], undecimated wavelet transform (UDWT) [15], "à-trous" wavelet transform (ATWT) [16], Laplacian pyramid [17], nonseparable transforms, either based on wavelets (e.g., curvelets [19]) or not (e.g., contourlets [18]). Hybrid methods have been also proposed, which use both component substitution and multiscale decomposition, such as guided filter PCA (GFPCA), described in Section II-C. The Bayesian approach relies on the use of posterior distribution of the full resolution target image given the observed MS and PAN images. This posterior, which is the Bayesian inference engine, has two factors: a) the likelihood function, which is the probability density of the observed MS and PAN images given the target image, and b) the prior probability density of the target image, which promotes target images with desired properties, such as being segmentally smooth. The selection of a suitable prior allows us to cope with the usual ill-posedness of the pansharpening inverse problems. The variational class is interpretable as particular case of the

Bayesian one, where the target image is estimated by maximizing the posterior probability density of the full resolution image. The works [20], [21], [22] are representative of the Bayesian and variational classes. As indicated in Table 1, the CS, MRA, and Hybrid classes of methods are detailed in Sections II-A, II-B, and II-C, respectively. Herein, the Bayesian class is not addressed in the MS+PAN context. It is addressed in detail, however, in Section II-D in the context of HS+PAN fusion.

With the increasing availability of HS systems, the pansharpening methods are now extended to the fusion of HS and panchromatic images [23], [24], [25], [26]. Pansharpening of HS images is still an open issue, and very few methods are presented in the literature to address it. The main advantage of HS image with respect to MS one is the more accurate spectral information they provide, which clearly benefits many applications such as unmixing [27], change detection [28], object recognition [29], scene interpretation [30] and classification [31]. Several of the methods designed for HS pansharpening were originally designed for the fusion of MS and HS data[32]–[36], the MS data constituting the high spatial resolution image. In this case, HS pansharpening can be seen as a particular case, where the MS image is composed of a single band, and thus reduces to a PAN image. In this paper, we divide these methods into two classes: Bayesian methods and matrix factorization based methods. In Section II-D, we briefly present the algorithms of [33], [36], and [35] of the former class and in Section II-E the algorithm of [32] of the latter class.

As one may expect, performing pansharpening with HS data is more complex than performing it with MS data. Whereas PAN and MS data are usually acquired almost in the same spectral range, the spectral range of an HS image normally is much wider than the one of the corresponding PAN image. Usually, the PAN spectral range is close to the visible spectral range of $0.4-0.8\mu$m (for example, the advanced land imager–ALI–instrument acquires PAN data in the range $0.48-0.69\mu$m). The HS range often covers the visible to the shortwave infrared (SWIR) range (for example, Hyperion acquires HS data in the range $0.4-2.5\mu$m, the range $0.8-2.5\mu$m being not covered by the PAN data). The difficulty that arises, consists in defining a fusion model that yields good results in the part of the HS spectral range that is not covered by PAN data, in which the high resolution spatial information is missing. This difficulty already existed, to some extent, in MS+PAN pansharpening, but it is much more severe in the HS+PAN case.

To the best of the authors' knowledge, there is currently no study comparing different fusion methods for HS data, particularly on datasets where the spectral domain of the HS image is larger than the one of the PAN image. This work aims at addressing this specific issue. The remainder of the paper is organized as follows. Section II reviews the methods under study, i.e., CS, MRA, hybrid, Bayesian, and matrix decomposition approaches. Section III summarizes the quality assessment measures that will be used to assess the image fusion results. Experimental results are presented in Section IV. Conclusions are drawn in Section V.

## II. HYPERSPECTRAL PANSHARPENING TECHNIQUES

This section presents some of the most relevant methods for HS pansharpening. First, we focus on the adaptation of the popular CS and MRA MS pansharpening methods for HS pansharpening. Later, we consider more recent methods based on Bayesian and matrix factorization approaches. A toolbox containing MATLAB implementations of these algorithms can be found online[1].

Before presenting the different methods, we introduce notation used along the paper. Bold-face capital letters refer to matrices and bold-face lower-case letters refer to vectors. The notation $\mathbf{X}^k$ refers to the $k$th row of $\mathbf{X}$. The operator $()^T$ denotes the transposition operation. Images are represented by matrices, in which each row corresponds to a spectral band, containing all the pixels of that band arranged in lexicographic order. We use the following specific matrices:

- $\mathbf{X} = [\boldsymbol{x}_1, \ldots, \boldsymbol{x}_n] \in \mathbb{R}^{m_\lambda \times n}$ represents the full resolution target image with $m_\lambda$ bands and $n$ pixels; $\widehat{\mathbf{X}}$ represents an estimate of that image.
- $\mathbf{Y}_H \in \mathbb{R}^{m_\lambda \times m}$, $\mathbf{Y}_M \in \mathbb{R}^{n_\lambda \times n}$, and $\mathbf{P} \in \mathbb{R}^{1 \times n}$ represents, respectively, the observed HS, MS, and PAN images, $n\lambda$ denoting the number of bands of the MS image and $m$ the total number of pixel in the $\mathbf{Y}_H$ image.
- $\widetilde{\mathbf{Y}}_H \in \mathbb{R}^{m_\lambda \times n}$ represents the HS images $\mathbf{Y}_H$ interpolated at the scale of the PAN image.

We denote by $d = \sqrt{m/n}$ the down-sampling factor, assumed to be the same in both spatial dimensions.

### A. COMPONENT SUBSTITUTION

CS approaches rely upon the projection of the higher spectral resolution image into another space, in order to

---

[1]http://openremotesensing.net

<table>
<tr><td colspan="2">

**TABLE 1. SUMMARY OF THE DIFFERENT CLASSES OF METHODS CONSIDERED IN THIS PAPER. WITHIN PARENTHESES, WE INDICATE THE ACRONYM OF EACH METHOD, FOLLOWED BY THE NUMBER OF THE SECTION IN WHICH THAT METHOD IS DESCRIBED.**

</td></tr>
<tr><td colspan="2">

**METHODS ORIGINALLY DESIGNED FOR MS PANSHARPENING**

</td></tr>
<tr><td>

**Component substitution** (CS, II-A)
Principal Component Analysis (PCA, II-A-1)
Gram Schmidt (GS, II-A-2)

</td><td>

**Multiresolution analysis** (MRA, II-B)
Smoothing filter-based intensity modulation (SFIM, II-B-1)
Laplacian pyramid (II-B-2)

</td></tr>
<tr><td>

**Hybrid methods** (II-C)
Guided Filter PCA (GFPCA)

</td><td>

**Bayesian methods**
*Not discussed in this paper*

</td></tr>
<tr><td colspan="2">

**METHODS ORIGINALLY DESIGNED FOR HS PANSHARPENING**

</td></tr>
<tr><td>

**Bayesian Methods** (II-D)
Naive Gaussian prior (II-D-1)
Sparsity promoting prior (II-D-2)
HySure (II-D-3)

</td><td>

**Matrix Factorization** (II-E)
Coupled Non-negative Matrix Factorization (CNMF)

</td></tr>
</table>

separate spatial and spectral information [6]. Subsequently, the transformed data are sharpened by substituting the component that contains the spatial information with the PAN image (or part of it). The greater the correlation between the PAN image and the replaced component, the less spectral distortion will be introduced by the fusion approach [6]. As a consequence, a histogram-matching procedure is often performed before replacing the PAN image. Finally, the CS-based fusion process is completed by applying the inverse spectral transformation to obtain the fused image.

The main advantages of the CS-based fusion techniques are the following: *i*) high fidelity in rendering the spatial details in the final image [37], *ii*) fast and easy implementation [8], and *iii*) robustness to misregistration errors and aliasing [38]. On the negative side, the main shortcoming of this class of techniques is the generation of a significant spectral distortion, cause by the spectral mismatch between the PAN and the HS spectral ranges [6].

Following [4], [39], a formulation of the CS fusion scheme is given by

$$\widehat{\mathbf{X}}^k = \widetilde{\mathbf{Y}}_H^k + g_k(\mathbf{P} - \mathbf{O}_L), \tag{1}$$

for $k = 1, \ldots, m_\lambda$, where $\widehat{\mathbf{X}}^k$ denotes the $k$th band of the estimated full resolution target image, $\mathbf{g} = [g_1, \ldots, g_{m_\lambda}]^T$ is a vector containing the *injection gains*, and $\mathbf{O}_L$ is defined as

$$\mathbf{O}_L = \sum_{i=1}^{m_\lambda} w_i \widetilde{\mathbf{Y}}_H^i, \tag{2}$$

where the weights $\mathbf{w} = [w_1, \ldots, w_i, \ldots, w_{m_\lambda}]^T$ measure the spectral overlap among the spectral bands and the PAN image [6], [40].

The CS family includes many popular pansharpening approaches. In [26], three approaches based on *principal component analysis* (PCA) [9] and *Gram-Schmidt* [13], [37] transformations have been compared for sharpening HS data. A brief description of these techniques follows.

*1) Principal Component Analysis:* PCA is a spectral transformation widely employed for pansharpening applications [9]. It is achieved through a rotation of the original data (i.e., a linear transformation) that yields the so-called principal components (PCs). The hypothesis underlying its application to pansharpening is that the spatial information (shared by all the channels) is concentrated in the first PC, while the spectral information (specific to each single band) is accounted for the other PCs. The whole fusion process can be described by the general formulation stated by Eqs. (1) and (2), where the vectors $\mathbf{w}$ and $\mathbf{g}$ of coefficient vectors are derived by the PCA procedure applied to the HS image.

*2) Gram-Schmidt:* The *Gram-Schmidt* transformation, often exploited in pansharpening approaches, was initially proposed in a patent by Kodak [13]. The fusion process starts by using, as the component, a synthetic low resolution PAN image $\mathbf{I}_L$ at the same spatial resolution as the HS

image[2]. A complete orthogonal decomposition is then performed, starting with that component. The pansharpening procedure is completed by substituting that component with the PAN image, and inverting the decomposition. This process is expressed by (1) using the gains [37]

$$g_k = \frac{\mathrm{cov}(\widetilde{\mathbf{Y}}_H^k, \mathbf{O}_L)}{\mathrm{var}(\mathbf{O}_L)} \tag{3}$$

for $k = 1, \ldots, m_\lambda$, where cov $(\cdot, \cdot)$ and var $(\cdot)$ denote the covariance and variance operations. Different algorithms are obtained by changing the definition of the weights in (2). The simplest way to obtain this low-resolution PAN image simply consists of averaging the HS bands (i.e., by setting $w_i = 1/m_\lambda$, for $i = 1, \ldots, m_\lambda$). In [37], the authors proposed an enhanced version, called *GS Adaptive* (*GSA*), in which $\mathbf{I}_L$ is generated by the linear model in (2) with weights estimated by the minimization of the mean square error between the estimated component and a filtered and downsampled version of the PAN image.

### B. MULTIRESOLUTION ANALYSIS

Pansharpening methods based on MRA apply a spatial filter to the PAN image for generating details to be injected into the HS data. The main advantages of the MRA-based fusion techniques are the following: *i*) temporal coherence [5] (see Sect.27.4.4), *ii*) spectral consistency, and *iii*) robustness to aliasing, under proper conditions [38]. On the negative side, the main shortcomings are *i*) the implementation is more complicated due to the design of spatial filters, *ii*) the computational burden is usually larger when compared to CS approaches. The fusion step is summarized as [4], [39]

$$\widehat{\mathbf{X}}^k = \widetilde{\mathbf{Y}}_H^k + \mathbf{G}_k \otimes (\mathbf{P} - \mathbf{P}_L), \tag{4}$$

for $k = 1, \ldots, m_\lambda$, where $\mathbf{P}_L$ denotes a low-pass version of $\mathbf{P}$, and the symbol $\otimes$ denotes element-wise multiplication. Furthermore, an equalization between the PAN image and the HS spectral bands is often required. $\mathbf{P} - \mathbf{P}_L$ is often called the *details* image, because it is a high-pass version of $\mathbf{P}$, and Eq. (4) can be seen as describing the way to *inject* details into each of the bands of the HS image. According to (4), the approaches belonging to this category can differ in *i*) the type of PAN low pass image $\mathbf{P}_L$ that is used, and *ii*) the definition of the gain coefficients $\mathbf{G}_k$. Two common options for defining the gains are:

1) $\mathbf{G}_k = \mathbb{1}$ for $k = 1, \ldots, m_\lambda$, where $\mathbb{1}$ is an appropriately sized matrix with all elements equal to 1. This choice identifies the so-called *additive* injection scheme;
2) $\mathbf{G}_k = \widetilde{\mathbf{Y}}_H^k \oslash \mathbf{P}_L$ for $k = 1, \ldots, m_\lambda$, where the symbol $\oslash$ denotes element-wise division. In this case, the details are weighted by the ratio between the upsampled HS image and the low-pass filtered PAN one, in order to reproduce the local intensity contrast of the PAN image

---

[2]GS is a more general method than PCA. PCA can be obtained, in GS, by using the first PC as the low resolution panchromatic image [41].

in the fused image [42]. This coefficient selection is often referred to as *high pass modulation* (HPM) method or *multiplicative* injection scheme. Some possible numerical issues could appear due to the division between $\widetilde{\mathbf{Y}}_H^k$ and $\mathbf{P}_L$ for low value of $\mathbf{P}_L$ creating fused pixel with very high value. In our toolbox this problem is addressed by clipping these values by using the information given by the dynamic range.

In the case of HS pansharpening, some further considerations should be taken into account. Indeed, the PAN and HS images are rarely acquired with the same platform. Thus, the ratio between the spatial resolutions of the PAN and HS images may not always be an integer number, or a power of two. This implies that some of the conventional approaches initially developed for MS images cannot be extended in a simple way to HS images (for example, dyadic wavelet-based algorithms cannot be applied in these conditions).

*1) Smoothing Filter-based Intensity Modulation (SFIM):* The direct implementation of Eq. (4) consists of applying a single linear time-invariant (LTI) low pass filter (LPF) $h_{LP}$ to the PAN image $\mathbf{P}$ for obtaining $\mathbf{P}_L$. Therefore, we have

$$\widehat{\mathbf{X}}^k = \widetilde{\mathbf{Y}}_H^k + g_k(\mathbf{P} - \mathbf{P} * h_{LP}) \tag{5}$$

for $k = 1, \ldots, m_\lambda$, where the symbol $*$ denotes the convolution operator. The SFIM algorithm [43] sets $h_{LP}$ to a simple box (i.e., an averaging) filter and exploits HPM as the details injection scheme.

*2) Laplacian Pyramid:* The low-pass filtering needed to obtain the signal $\mathbf{P}_L$ at the original HS scale can be performed in more than one step. This is commonly referred to as pyramidal decomposition and dates back to the seminal work of Burt and Adelson [17]. If a Gaussian filter is used to lowpass filter the images in each step, one obtains a so-called *Gaussian pyramid*. The differences between consecutive levels of a Gaussian pyramid define the so-called *Laplacian pyramid*. The suitability of the latter to the pansharpening problem has been shown in [44]. Indeed, Gaussian filters can be tuned to closely match the sensor modulation transfer function (MTF). In this case, the unique parameter that characterizes the whole distribution is the Gaussian's standard deviation, which is determined from sensor-based information (usually from the value of the amplitude response at the Nyquist frequency, provided by the manufacturer). Both *additive* and *multiplicative* details injection schemes have been used in this framework [42], [45]. They will be referred to as *MTF-Generalized Laplacian Pyramid* (MTF-GLP) [45] and *MTF-GLP with High Pass Modulation* (MTF-GLP-HPM) [42], respectively.

## C. HYBRID METHODS

Hybrid approaches use concepts from different classes of methods, namely from CS and MRA ones, as explained next.

*1) Guided Filter PCA (GFPCA):* One of the main challenges for fusing low-resolution HS and high-resolution PAN/RGB data is to find an appropriate balance between spectral and spatial preservation. Recently, the guided filter [46] has been used in many applications (e.g. edge-aware smoothing and detail enhancement), because of its efficiency and strong ability to transfer the structures of the guidance image to the filtering output. Its application to HS data can be found in [47], where the guided filter was applied to transfer the structures of the principal components of the HS image to the initial classification maps.

Here, we briefly describe an image fusion framework which uses a guided filter in the PCA domain (GFPCA) [48]. The approach won the "Best Paper Challenge" award at the 2014 IEEE data fusion contest [48], by fusing a low spatial resolution thermal infrared HS image and a high spatial resolution, visible RGB image associated with the same scene. Fig. 1 shows the framework of GFPCA. Instead of using CS, which may cause spectral distortions, GFPCA uses a high resolution PAN/RGB image to guide the filtering process aimed at obtaining super-resolution. In this way, GFPCA does not only preserve the spectral information from the original HS image, but also transfers the spatial structures of the high resolution PAN/RGB image to the enhanced HS image. To speed up the processing, GFPCA first uses PCA to decorrelate the bands of the HS image, and to separate the information content from the noise. The first $p \ll m_\lambda$ PCA channels contain most of the energy (and most of the information) of an HS image, and the remaining $m_\lambda - p$ PCA channels mainly contain noise (recall that $m_\lambda$ is the number of spectral bands of the HS image). When applied to these noisy (and numerous) $m_\lambda - p$ channels, the guided filter amplifies the noise and causes a high computational cost in processing the data, which is undesirable. Therefore, guided filtering is used to enlarge only the first $k$ PCA channels, preserving the structures of the PAN/RGB image, while cubic interpolation is used to upsample the remaining channels.

> **DERIVED FROM THE STANDARD PANSHARPENING LITERATURE, COMPONENT SUBSTITUTION, MULTIRESOLUTION ANALYSIS AND HYBRID METHODS ARE THE THREE MAIN CLASSES OF METHODS.**
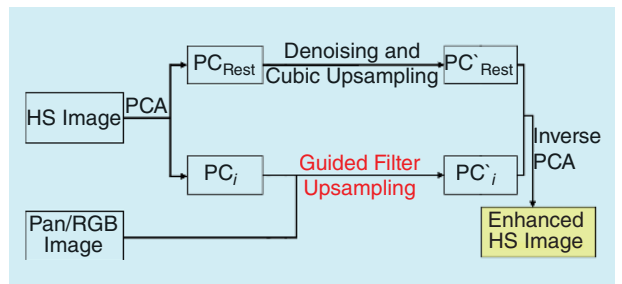


**FIGURE 1.** Fusion of HS and PAN/RGB images with the GFPCA framework.

Let $PC_i$, with $(i \le p)$, denote the $i$th PC channel obtained from the HS image $\mathbf{Y}_H$, with its resolution increased to that of the guided image $\mathbf{Y}$ ($\mathbf{Y}$ may be a PAN or an RGB image) through bicubic interpolation. The output of the filtering, $PC_i'$, can be represented as an affine transformation of $\mathbf{Y}$ in a local window $\omega_j$ of size $(2d+1) \times (2d+1)$ as follows:

$$PC_i' = a_j \mathbf{Y} + b_j, \quad \forall i \in \omega_j. \tag{6}$$

The above model ensures that the output $PC_i'$ has an edge only if the guided image $\mathbf{Y}$ has an edge, since $\nabla(PC_i') = a\nabla\mathbf{Y}$. The following cost function is used to determine the coefficients $a_j$ and $b_j$:

$$E(a_j, b_j) = \sum_{i \in \omega_j} [(a_j \mathbf{Y} + b_j - PC_i)^2 + \epsilon a_j^2], \tag{7}$$

where $\epsilon$ is a regularization parameter determining the degree of blurring for the guided filter. For more details about the guided filtering scheme, we invite the reader to consult [46]. The cost function $E$ leads the term $a_j \mathbf{Y} + b_j$ to be as close as possible to $PC_i$, in order to ensure the preservation of the original spectral information. Before applying inverse PCA, GFPCA also removes the noise from the remaining PCA channels $PC_{Rest}$ using a soft-thresholding scheme (similarly to [49]), and increases their spatial resolution to the resolution of the PAN/RGB image using cubic interpolation only (without guided filtering).

### D. BAYESIAN APPROACHES

The fusion of HS and high spatial resolution images, e.g., MS or PAN images, can be conveniently formulated within the Bayesian inference framework. This formulation allows an intuitive interpretation of the fusion process via the posterior distribution of the Bayesian fusion model. Since the fusion problem is usually ill-posed, the Bayesian methodology offers a convenient way to regularize the problem by defining an appropriate prior distribution for the scene of interest. Following this strategy, different Bayesian estimators for fusing co-registered high spatial-resolution MS and high spectral-resolution HS images have been designed [33]–[36], [50]–[54]. The observation models associated with the HS and MS images can be written as follows [50], [55], [56]

$$\begin{aligned} \mathbf{Y}_H &= \mathbf{XBS} + \mathbf{N}_H \\ \mathbf{Y}_M &= \mathbf{RX} + \mathbf{N}_M \end{aligned} \tag{8}$$

where $\mathbf{X}$, $\mathbf{Y}_H$, and $\mathbf{Y}_M$ were defined in Section II, and

- $\mathbf{B} \in \mathbb{R}^{n \times n}$ is a cyclic convolution operator, corresponding to the spectral response of the HS sensor expressed in the resolution of the MS or PAN image,
- $\mathbf{S} \in \mathbb{R}^{n \times m}$ is a down-sampling matrix with down-sampling factor $d$,
- $\mathbf{R} \in \mathbb{R}^{n_\lambda \times m_\lambda}$ is the spectral response of the MS or PAN sensor,
- $\mathbf{N}_H$ and $\mathbf{N}_M$ are the HS and MS noises, assumed to have zero mean Gaussian distributions with covariance matrices $\mathbf{\Lambda}_H$ and $\mathbf{\Lambda}_M$, respectively.

For the sake of generality, the formulation in this section assumes that the observed data is the pair of matrices $(\mathbf{Y}_H, \mathbf{Y}_M)$. Since a PAN image can be represented by $\mathbf{Y}_M$ with $n_\lambda = 1$, the observation model (8) covers the HS+PAN fusion problem considered in this paper.

Using geometrical considerations well grounded in the HS imaging literature devoted to the linear unmixing problem [27], the high spatial resolution HS image to be estimated is assumed to live in a low dimensional subspace. This hypothesis is very reliable when the observed scene is composed of a finite number of macroscopic materials (called *endmembers*). Based on the model (8) and on the low dimensional subspace assumptions, the distributions of $\mathbf{Y}_H$ and $\mathbf{Y}_M$ can be expressed as follows

$$\begin{aligned} \mathbf{Y}_H \mid \mathbf{U} &\sim \mathcal{MN}_{m_\lambda, m}(\mathbf{HUBS}, \Lambda_H, \mathbf{I}_m), \\ \mathbf{Y}_M \mid \mathbf{U} &\sim \mathcal{MN}_{n_\lambda, n}(\mathbf{RHU}, \Lambda_M, \mathbf{I}_n) \end{aligned} \tag{9}$$

where $\mathcal{MN}$ represents the matrix normal distribution [57], the target image is $\mathbf{X} = \mathbf{HU}$, with $\mathbf{H} \in \mathbb{R}^{m_\lambda \times \widetilde{m_\lambda}}$ containing in its columns a basis of the signal subspace of size $\widetilde{m_\lambda} \ll m_\lambda$ and $\mathbf{U} \in \mathbb{R}^{\widetilde{m_\lambda} \times n}$ contains the representation coefficients of $\mathbf{X}$ with respect to $\mathbf{H}$. The subspace transformation matrix $\mathbf{H}$ can be obtained via different approaches, e.g., PCA [58] or vertex component analysis [59].

According to Bayes' theorem and using the fact that the noises $\mathbf{N}_H$ and $\mathbf{N}_M$ are independent, the posterior distribution of $\mathbf{U}$ can be written as

$$p(\mathbf{U} \mid \mathbf{Y}_H, \mathbf{Y}_M) \propto p(\mathbf{Y}_H \mid \mathbf{U})p(\mathbf{Y}_M \mid \mathbf{U})p(\mathbf{U}) \tag{10}$$

or equivalently[3]

$$-\log p(\mathbf{U} \mid \mathbf{Y}_H, \mathbf{Y}_M) \doteq \underbrace{\frac{1}{2}\left\|\mathbf{\Lambda}_H^{-\frac{1}{2}}(\mathbf{Y}_H - \mathbf{HUBS})\right\|_F^2}_{\substack{\text{HS data term} \\ \doteq \log p(\mathbf{Y}_H \mid \mathbf{U})}} +$$

$$\underbrace{\frac{1}{2}\left\|\mathbf{\Lambda}_M^{-\frac{1}{2}}(\mathbf{Y}_M - \mathbf{RHU})\right\|_F^2}_{\substack{\text{MS data term} \\ \doteq \log p(\mathbf{Y}_M \mid \mathbf{U})}} + \underbrace{\lambda\phi(\mathbf{U})}_{\substack{\text{regularizer} \\ \doteq \log p(\mathbf{U})}} \tag{11}$$

where $\|\mathbf{X}\|_F \overset{\text{def}}{=} \sqrt{\text{Tr}(\mathbf{XX}^T)}$ is the Frobenius norm of $\mathbf{X}$. An important quantity in the negative log-posterior (11) is the penalization term $\phi(\mathbf{U})$ which allows the inverse problem (8) to be regularized. The next sections discuss different ways of defining this penalization term.

*1) Naive Gaussian prior:* Denote as $\mathbf{u}_i(i = 1, \ldots, n)$ the columns of the matrix $\mathbf{U}$ that are assumed to be mutually independent and are assigned the following Gaussian prior distributions

$$p(\mathbf{u}_i \mid \boldsymbol{\mu}_i, \boldsymbol{\Sigma}_i) = \mathcal{N}(\boldsymbol{\mu}_i, \boldsymbol{\Sigma}_i) \tag{12}$$

---

[3]We use the symbol $\doteq$ to denote equality apart from an additive constant. The additive constants are irrelevant, since the functions under consideration are to be optimized, and the additive constants do not change the locations of the optima.

where $\boldsymbol{\mu}_i$ is a fixed image defined by the interpolated HS image projected into the subspace of interest, and $\boldsymbol{\Sigma}_i$ is an unknown hyperparameter matrix. Different interpolations can be investigated to build the mean vector $\boldsymbol{\mu}_i$. In this paper, we have followed the strategy proposed in [50]. To reduce the number of parameters to be estimated, the matrices $\boldsymbol{\Sigma}_i$ are assumed to be identical, i.e., $\boldsymbol{\Sigma}_1 = \cdots = \boldsymbol{\Sigma}_n = \boldsymbol{\Sigma}$. The hyperparameter $\boldsymbol{\Sigma}$ is assigned a proper prior and is estimated jointly with the other parameters of interest. To infer the parameter of interest, namely the projected highly resolved HS image $\mathbf{U}$, from the posterior distribution $p(\mathbf{U} \mid \mathbf{Y}_H, \mathbf{Y}_M)$, several algorithms have been proposed. In [33], [34], a Markov chain Monte Carlo (MCMC) method is exploited to generate a collection of $N_{MC}$ samples that are asymptotically distributed according to the target posterior. The corresponding Bayesian estimators can then be approximated using these generated samples. For instance, the minimum mean square error (MMSE) estimator of $\mathbf{U}$ can be approximated by an empirical average of the generated samples $\widehat{\mathbf{U}}_{MMSE} \approx 1/(N_{MC} - N_{bi}) \sum_{t=N_{bi}+1}^{N_{MC}} \mathbf{U}^{(t)}$, where $N_{bi}$ is the number of burn-in iterations required to reach the sampler convergence, and $\mathbf{U}^{(t)}$ is the image generated in the $t$th iteration. The highly-resolved HS image can finally be computed as $\widehat{\mathbf{X}}_{MMSE} = \mathbf{H}\widehat{\mathbf{U}}_{MMSE}$. An extension of the proposed algorithm has been proposed in [53] to handle the specific scenario of an unknown sensor spectral response. In [60], a deterministic counterpart of this MCMC algorithm has been developed, where the Gibbs sampling strategy of [33] has been replaced with a block coordinate descent method to compute the maximum a posteriori (MAP) estimator. Finally, very recently, a Sylvester equation-based explicit solution of the related optimization problem has been derived in [61], [87] leading to a significant decrease of the computational complexity.

*2) Sparsity promoted Gaussian prior:* Instead of incorporating a simple Gaussian prior or smooth regularization for the HS and MS fusion [34], [50], [51], a sparse representation can be used to regularize the fusion problem. More specifically, image patches of the target image (projected onto the subspace defined by $\mathbf{H}$) are represented as a sparse linear combination of elements from an appropriately chosen over-complete dictionary with columns referred to as atoms. Learning the dictionary from the observed images instead of using predefined bases [62]–[64] generally improves image representation [65], which is preferred in most scenarios. Therefore, an adaptive sparse image-dependent regularization can be explored to solve the fusion problem (8). In [36], the following regularization term was introduced:

$$\phi(\mathbf{U}) \propto -\log p(\mathbf{U}) \doteq \frac{1}{2} \sum_{k=1}^{\tilde{m}_\lambda} \left\| \mathbf{U}_k - \mathcal{P}(\bar{\mathbf{D}}_k \bar{\mathbf{A}}_k) \right\|_F^2, \quad (13)$$

where

- $\mathbf{U}_k \in \mathbb{R}^n$ is the $k$th band (or row) of $\mathbf{U} \in \mathbb{R}^{\tilde{m}_\lambda \times n}$, with $k = 1, \ldots, \tilde{m}_\lambda$,

- $\mathcal{P}(\cdot): \mathbb{R}^{n_p \times n_{pat}} \mapsto \mathbb{R}^{n \times 1}$ is a linear operator that averages the overlapping patches[4] of each band, $n_{pat}$ being the number of patches associated with the $i$th band,
- $\bar{\mathbf{D}}_k \in \mathbb{R}^{n_p \times n_{at}}$ is the overcomplete dictionary of the ith band, whose columns are basis elements of size $n_p$ (corresponding to the size of a patch), $n_{at}$ being the number of dictionary atoms, and
- $\bar{\mathbf{A}}_k \in \mathbb{R}^{n_{at} \times n_{pat}}$ is the code of the $i$th band.

Inspired by hierarchical models frequently encountered in Bayesian inference [67], a second level of hierarchy can be considered in the Bayesian paradigm by including the code $\mathbf{A}$ within the estimation, while fixing the support $\bar{\Omega} \triangleq \{\bar{\Omega}_1, \ldots, \bar{\Omega}_{\tilde{m}_\lambda}\}$ of the code $\mathbf{A}$. Once $\bar{\mathbf{D}}, \bar{\Omega}$ and $\mathbf{H}$ have been learned from the HS and MS data, maximizing the posterior distribution of $\mathbf{U}$ and $\mathbf{A}$ reduces to a standard constrained quadratic optimization problem with respect to $\mathbf{U}$ and $\mathbf{A}$. The resulting optimization problem is difficult to solve due to its large dimension and due to the fact that the linear operators $\mathbf{H}(\cdot)\mathbf{BD}$ and $\mathcal{P}(\cdot)$ cannot be easily diagonalized. To cope with this difficulty, an optimization technique that alternates minimization $\mathbf{U}$ and $\mathbf{A}$ has been introduced in [36] (where details on the learning of $\bar{\mathbf{D}}, \bar{\Omega}$ and $\mathbf{H}$ can be found). In [61], the authors show that the minimization w.r.t. $\mathbf{U}$ can be achieved analytically, which greatly accelerates the fusion process.

*3) HySure:* The works [35], [54] introduce a convex regularization problem which can be seen under a Bayesian framework. The proposed method uses a form of vector total variation (VTV) [68] for the regularizer $\phi(\mathbf{U})$, taking into account both the spatial and the spectral characteristics of the data. In addition, another convex problem is formulated to estimate the relative spatial and spectral responses of the sensors $\mathbf{B}$ and $\mathbf{R}$ from the data themselves. Therefore, the complete methodology can be classified as a blind superresolution method, which, in contrast to the classical blind linear inverse problems, is tackled by solving two convex problems.

The VTV regularizer (see [68]) is given by

$$\phi(\mathbf{U}) = \sum_{j=1}^{n} \sqrt{\sum_{k=1}^{\tilde{m}_\lambda} \left\{ [(\mathbf{UD}_h)_j^k]^2 + [(\mathbf{UD}_v)_j^k]^2 \right\}}, \quad (14)$$

where $\mathbf{A}_j^k$ denotes the element in the $k$th row and $j$th column of matrix $\mathbf{A}$, and the products by matrices $\mathbf{D}_h$ and $\mathbf{D}_v$ compute the horizontal and vertical discrete differences of an image, respectively, with periodic boundary conditions.

The HS pansharpened image is the solution to the following optimization problem

$$\underset{\mathbf{U}}{\text{minimize}} \quad \frac{1}{2} \| \mathbf{Y}_H - \mathbf{HUBS} \|_F^2 + \frac{\lambda_m}{2} \| \mathbf{Y}_M - \mathbf{RHU} \|_F^2 + \lambda_\phi \phi(\mathbf{U}), \quad (15)$$

where $\lambda_m$ and $\lambda_\phi$ control the relative weights of the different terms. The optimization problem (15) is hard to solve, essentially for three reasons: the downsampling operator

---

[4]A decomposition into overlapping patches was adopted, to prevent the occurrence of blocking artifacts [66].

**BS** is not diagonalizable, the regularizer $\phi(\mathbf{U})$ is nonquadratic and nonsmooth, and the target image has a very large size. These difficulties were tackled by solving the problem via the split augmented lagrangian shrinkage algorithm (SALSA) [69], an instance of ADMM. As an alternative, the main step of the ADMM scheme can be conducted using an explicit solution of the corresponding minimization problem, following the strategy in [61].

The relative spatial and spectral responses **B** and **R** were estimated by solving the following optimization problem:

$$\underset{\mathbf{B},\mathbf{R}}{\text{minimize}} \quad \|\mathbf{R}\mathbf{Y}_H - \mathbf{Y}_M\mathbf{B}\mathbf{S}\|^2 + \lambda_B\phi_B(\mathbf{B}) + \lambda_R\phi_R(\mathbf{R}) \quad (16)$$

where $\phi_B(\cdot)$ and $\phi_R(\cdot)$ are quadratic regularizers and $\lambda_B, \lambda_R \geq 0$ are their respective regularization parameters.

### E. MATRIX FACTORIZATION

The matrix factorization approach for HS+MS fusion essentially exploits two facts: 1) A basis or dictionary **H** for the signal subspace can be learned from the HS observed image $\mathbf{Y}_H$, yielding the factorization $\mathbf{X} = \mathbf{H}\mathbf{U}$; 2) using this decomposition in the second equation of (8) and for negligible noise, i.e., $\mathbf{N}_M \simeq 0$, we have $\mathbf{Y}_H = \mathbf{R}\mathbf{H}\mathbf{U}$. Assuming that the columns of **RH** are full rank or that the columns of **U** admit a sparse representation w.r.t. the columns of **RH**, then we can recover the true solution, denoted by $\widehat{\mathbf{U}}$, and use it to compute the target image as $\widehat{\mathbf{X}} = \mathbf{H}\widehat{\mathbf{U}}$. The works [32], [70]–[74] are representative of this line of attack. In what follow, we detail the application of the coupled nonnegative matrix factorization (CNMF) [32] to the HS+PAN fusion problem.

The CNMF was proposed for the fusion of low spatial resolution HS and high spatial resolution MS data to produce fused data with high spatial and spectral resolutions [32]. It is applicable to HS pansharpening as a special case, in which the higher spatial resolution image has a single band [75]. CNMF alternately unmixes both sources of data to obtain the endmember spectra and the high spatial resolution abundance maps.

To describe this method, it is convenient to first briefly introduce linear mixture models for HS images. These models are commonly used for spectral unmixing, owing to their physical effectiveness and mathematical simplicity [27]. The spectrum at each pixel is assumed to be a linear combination of several endmember spectra. Therefore, $\mathbf{X} \in \mathbb{R}^{m_\lambda \times n}$ is formulated as

$$\mathbf{X} = \mathbf{H}\mathbf{U} \quad (17)$$

where $\mathbf{H} \in \mathbb{R}^{m_\lambda \times p}$ is the signature matrix, containing the spectral representations of the endmembers, and $\mathbf{U} \in \mathbb{R}^{p \times n}$ is the abundance matrix, containing the relative abundances of the different endmembers at the various pixels, with $p$ representing the number of endmembers. By substituting (17) into (8), $\mathbf{Y}_H$ and $\mathbf{Y}_M$ can be approximated as

$$\mathbf{Y}_H \approx \mathbf{H}\mathbf{U}_H$$
$$\mathbf{Y}_M \approx \mathbf{H}_M\mathbf{U} \quad (18)$$

where $\mathbf{U}_H = \mathbf{U}\mathbf{B}\mathbf{S}$ and $\mathbf{H}_M = \mathbf{R}\mathbf{H}$. CNMF alternately unmixes $\mathbf{Y}_H$ and $\mathbf{Y}_M$ in the framework of nonnegative matrix factorization (NMF) [76] to estimate **H** and **U** under the constraints of the relative sensor characteristics. CNMF starts with NMF unmixing of the low spatial resolution HS data. The matrix **H** can be initialized using, for example, the vertex component analysis (VCA) [59], and **H** and $\mathbf{U}_H$ are then alternately optimized by minimizing $\|\mathbf{Y}_H - \mathbf{H}\mathbf{U}_H\|_F^2$ using Lee and Seung's multiplicative update rules [76]. Next, **U** is estimated from the higher spatial resolution data. $\mathbf{H}_M$ is set to **RH** and **U** is initialized by the spatially up-sampled matrix of $\mathbf{U}_H$ obtained by using bilinear interpolation. For HS pansharpening ($n_\lambda = 1$), only **U** is optimized by minimizing $\|\mathbf{Y}_M - \mathbf{H}_M\mathbf{U}\|_F^2$ with the multiplicative update rule, whereas both $\mathbf{H}_M$ and **U** are alternately optimized in the case of HS+MS data fusion. Finally, the high spatial resolution HS data can be obtained by the multiplication of **H** and **U**. The abundance sum-to-one constraint is implemented using a method given in [77], where the data and signature matrices are augmented by a row of constants. The relative sensor characteristics, such as **BS** and **R**, can be estimated from the observed data sources [78].

## III. QUALITY ASSESSMENT OF FUSION PRODUCTS

Quality assessment of a pansharpened real-life HS image is not an easy task [79], [9], since a reference image is generally not available. When such an image is not available, two kinds of comparisons can be performed: i) Each band of the fused image can be compared with the PAN image, with an appropriate criterion. The PAN image can also be compared with the PAN image reconstructed from the fused image. ii) The fused image can be spatially degraded to the resolution of the original HS image. The two images can then be compared, to assess to what extent the spectral information has been modified by the fusion method.

In order to be able to use a reference image for quality assessment, one normally has to resort to the use of semi-synthetic HS and PAN images. In this case, a real-life HS image is used as reference. The HS and PAN images to be processed are obtained by degrading this reference image. A common methodology for obtaining the degraded images is Wald's protocol, described in the next subsection. In order to evaluate the quality of the fused image with respect to the reference image, a number of statistical measures can be computed. The most widely used ones are described ahead, and used in the experiments reported in Section IV-B.

### A. WALD'S PROTOCOL

A general paradigm for quality assessment of fused images that is usually accepted in the research community was first proposed by Wald *et al.* [79]. This paradigm is based on two properties that the fused data have to have, as much as possible, namely consistency and synthesis properties. The

first property requires the reversibility of the pansharpening process: it states that the original HS image should be obtained by properly degrading the pansharpened image. The second property requires that the pansharpened image be as similar as possible to the image of the same scene that would be obtained, by the same sensor, at the higher resolution. This condition entails that both the features of each single band and the mutual relations among bands have to be preserved. However, the definition of an assessment method that fulfills these constraints is still an open issue [80], [81], and closely relates to the general discussion regarding image quality assessment [82] and image fusion [83], [84].

Wald's protocol for assessing the quality of pansharpening methods [79], depicted in Fig. 2, synthetically generates simulated observed images from a reference HS image, and then evaluates the pansharpening methods' results against that reference image. The protocol consists of the following steps:

▶ Given a HS image, $\mathbf{X}$, to be used as reference, a simulated observed low spatial resolution HS image, $\mathbf{Y}_H$, is obtained by applying a Gaussian blurring to $\mathbf{X}$, and then downsampling the result by selecting one out of every $d$ pixels in both the horizontal and vertical directions, where $d$ denotes the downsampling factor.

▶ A simulated PAN image, $\mathbf{P}$, is obtained by multiplying the reference HS image, on the left, by a suitably chosen spectral response vector, $\mathbf{P} = \mathbf{r}^T \mathbf{X}$.

▶ The pansharpening method to be evaluated is applied to the simulated observations $\mathbf{Y}_H$ and $\mathbf{P}$, yielding the estimated superresolution HS image, $\widehat{\mathbf{X}}$.

▶ Finally, the estimated superresolution HS image and the reference one are compared, to obtain quantitative quality measures.

## B. QUALITY MEASURES

Several quality measures have been defined in the literature, in order to determine the similarity between estimated and reference spectral images. These measures can be generally classified into three categories, depending on whether they attempt to measure the spatial, spectral or global quality of the estimated image. This review is limited to the most widely used quality measures, namely the *cross correlation* (CC), which is a spatial measure, the *spectral angle mapper* (SAM), which is a spectral measure, and the *root mean squared error* (RMSE) and *erreur relative globale adimensionnelle de synthèse* (ERGAS) [85], which are global measures. Below we provide the formal definitions of these measures operating on the estimated image $\widehat{\mathbf{X}} \in \mathbb{R}^{m_\lambda \times n}$ and on the reference HS image $\mathbf{X} \in \mathbb{R}^{m_\lambda \times n}$. In the definitions, $\widehat{\mathbf{x}}_j$ and $\mathbf{x}_j$ denote the $j$th columns of $\widehat{\mathbf{X}}$ and $\mathbf{X}$, respectively, the matrices $\mathbf{A}, \mathbf{B} \in \mathbb{R}^{1 \times n}$ denote two generic single-band images, and $\mathbf{A}_i$ denotes the $i$th element of $\mathbf{A}$.

*1) Cross correlation*: The CC, which characterizes the geometric distortion, is defined as

$$\mathrm{CC}(\widehat{\mathbf{X}}, \mathbf{X}) = \frac{1}{m_\lambda} \sum_{i=1}^{m_\lambda} \mathrm{CCS}(\widehat{\mathbf{X}}^i, \mathbf{X}^i), \tag{19}$$

where CCS is the cross correlation for a single-band image, defined as

$$\mathrm{CCS}(\mathbf{A}, \mathbf{B}) = \frac{\sum_{j=1}^{n} (\mathbf{A}_j - \mu_A)(\mathbf{B}_j - \mu_B)}{\sqrt{\sum_{j=1}^{n} (\mathbf{A}_j - \mu_A)^2 \sum_{j=1}^{n} (\mathbf{B}_j - \mu_B)^2}},$$

where, $\mu_A = (1/n) \sum_{j=1}^{n} \mathbf{A}_j$ is the sample mean of $\mathbf{A}$. The ideal value of CC is 1.

*2) Spectral angle mapper*: The SAM, which is a spectral measure, is defined as

$$\mathrm{SAM}(\widehat{\mathbf{X}}, \mathbf{X}) = \frac{1}{n} \sum_{j=1}^{n} \mathrm{SAM}(\widehat{\mathbf{x}}_j, \mathbf{x}_j), \tag{20}$$

where, given the vectors $\mathbf{a}, \mathbf{b} \in \mathbb{R}^{m_\lambda}$,

$$\mathrm{SAM}(\mathbf{a}, \mathbf{b}) = \arccos\left(\frac{\langle \mathbf{a}, \mathbf{b} \rangle}{\|\mathbf{a}\| \|\mathbf{b}\|}\right), \tag{21}$$

$\langle \mathbf{a}, \mathbf{b} \rangle = \mathbf{a}^T \mathbf{b}$ is inner product between $\mathbf{a}$ and $\mathbf{b}$, and $\| \cdot \|$ is the $\ell_2$ norm. The SAM is a measure of the spectral shape preservation. The optimal value of SAM is 0. The values of SAM reported in our experiments have been obtained by averaging the values obtained for all the image pixels.

*3) Root mean squared error*: The RMSE measures the $\ell_2$ error between the two matrices $\mathbf{X}$ and $\widehat{\mathbf{X}}$

$$\mathrm{RMSE}(\widehat{\mathbf{X}}, \mathbf{X}) = \frac{\|\widehat{\mathbf{X}} - \mathbf{X}\|_F}{\sqrt{n * m_\lambda}} \tag{22}$$
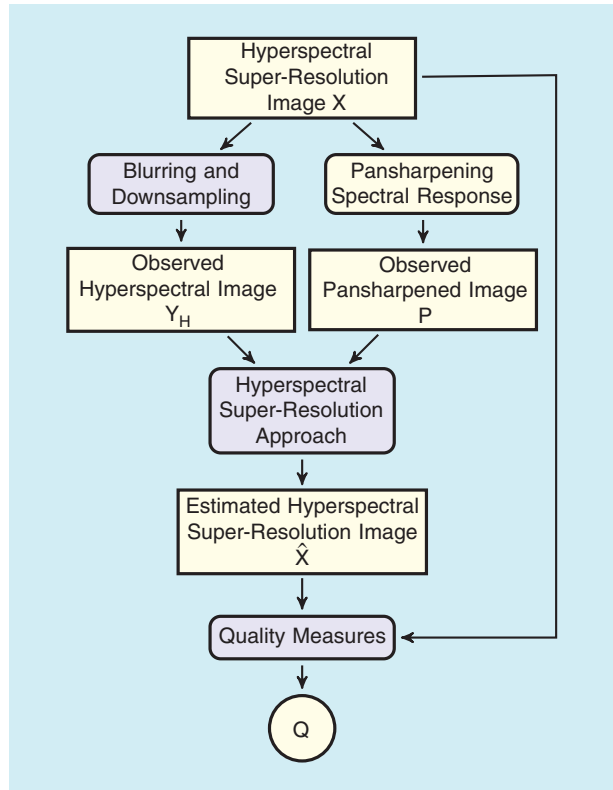


**FIGURE 2.** Flow diagram of the experimental methodology, derived from Wald's protocol (simulated observations), for synthetic and semi-real datasets.

where $\| \mathbf{X} \|_F = \sqrt{\operatorname{trace}(\mathbf{X}^T\mathbf{X})}$ is the Frobenius norm of $\mathbf{X}$. The ideal value of RMSE is 0.

*4) Erreur relative globale adimensionnelle de synthèse*: ERGAS offers a global indication of the quality of a fused image. It is defined as

$$\text{ERGAS}(\widehat{\mathbf{X}}, \mathbf{X}) = 100d \sqrt{\frac{1}{m_\lambda} \sum_{k=1}^{m_\lambda} \left( \frac{\text{RMSE}_k}{\mu_k} \right)^2}, \qquad (23)$$

where $d$ is the ratio between the linear resolutions of the PAN and HS images, defined as

$$d = \frac{\text{PAN linear spatial resolution}}{\text{HS linear spatial resolution}},$$

$\text{RMSE}_k = \left( \| \widehat{X}^k - X^k \|_F / \sqrt{n} \right)$, and $\mu_k$ is the sample mean of the $k$th band of $\mathbf{X}$. The ideal value of ERGAS is 0.

## IV. EXPERIMENTAL RESULTS

### A. DATASETS

The datasets that were used in the experimental tests were all semi-synthetic, generated according to the Wald's protocol. In all cases, the spectral bands corresponding to the absorption band of water vapor, and the bands that were too noisy, were removed from the reference image before further processing. Three real-life HS images have been used as reference images for the Wald's protocol. In the following, we describe the datasets that were generated from these images. Table 2 summarizes their properties. These datasets are expressed in spectral luminance (nearest to the sensor output, without pre-processing) and are correctly registered.

1) *Moffett field dataset*: This dataset represents a mixed urban/rural scene. The dimensions of the PAN are $185 \times 395$ with a spatial resolution of 20m whereas the size of the HS image is $37 \times 79$ with a spatial resolution of 100m (which means a spatial resolution ratio of 5 between the two images). The HS image has been acquired by the airborne hyperspectral instrument airborne visible infrared image spectrometer (AVIRIS). This instrument is characterized by 224 bands covering the spectral range 0.4–2.5μm.

2) *Camargue dataset*: This dataset represents a rural area with different kinds of crops. The dimensions of the PAN image are $500 \times 500$ with a spatial resolution of 4m whereas the size of the HS image is $100 \times 100$ with a spatial resolution of 20m, (which means a spatial resolution ratio of 5 between the two images). The HS image has been acquired by the airborne hyperspectral instrument HyMap (Hyperspectral Mapper) in 2007. The hyperspectral instrument is characterized by 125 bands covering the spectral range 0.4–2.5μm.

3) *Garons dataset*: This dataset represents a rural area with a small village. The dimension of the PAN image are $400 \times 400$ with a spatial resolution of 4m whereas the size of the HS image is $80 \times 80$ with a spatial resolution of 20m, (which means a spatial resolution ratio of 5 between the two images). This dataset has been acquired with the HyMap instrument in 2009.

### B. RESULTS AND DISCUSSION

Methods presented in Section II have been applied on the three datasets presented in Section IV-A and analyzed following the Wald's Protocol (Section III-B). Tables 3, 4, 5 report their quantitative evaluations with respect to the quality measures detailed in Section III-B.

Figures 3, 4, and 5 represent the RMSEs per pixel between the image estimated by some methods and the reference

**TABLE 2. CHARACTERISTIC OF THE THREE DATASETS.**

| DATASET | DIMENSIONS | SPATIAL RES | N | INSTRUMENT |
|---------|------------|-------------|---|------------|
| Moffett | PAN $185 \times 395$ | 20m | 224 | AVIRIS |
|  | HS $37 \times 79$ | 100m |  |  |
| Camargue | PAN $500 \times 500$ | 4m | 125 | HyMap |
|  | HS $100 \times 100$ | 20m |  |  |
| Garons | PAN $400 \times 400$ | 4m | 125 | HyMap |
|  | HS $80 \times 80$ | 20m |  |  |

**TABLE 3. QUALITY MEASURES FOR THE MOFFETT FIELD DATASET.**

| METHOD | CC | SAM | RMSE | ERGAS |
|--------|------|------|-------|-------|
| SFIM | 0.96762 | 7.8313 | 257.6388 | 4.6072 |
| MTF-GLP | 0.97148 | 6.9604 | 253.5582 | 4.2867 |
| MTF-GLP-HPM | 0.96925 | 7.7301 | 260.9860 | 4.5329 |
| GS | 0.91722 | 12.9589 | 420.5469 | 7.2204 |
| GSA | 0.95304 | 10.4024 | 325.1781 | 5.5938 |
| PCA | 0.90664 | 13.4512 | 445.1298 | 7.6215 |
| GFPCA | 0.91614 | 11.3363 | 404.2979 | 7.0619 |
| CNMF | 0.95633 | 9.0464 | 309.9017 | 5.3469 |
| Bayesian Naive | 0.97785 | 7.1308 | 220.0310 | 3.7807 |
| Bayesian Sparse | **0.98170** | **6.6253** | **200.1856** | **3.4262** |
| HySure | 0.97086 | 7.3508 | 253.0972 | 4.3315 |

**TABLE 4. QUALITY MEASURES FOR THE CAMARGUE DATASET.**

| METHOD | CC | SAM | RMSE | ERGAS |
|--------|------|------|-------|-------|
| SFIM | 0.95296 | 3.6067 | 488.4061 | 2.6419 |
| MTF-GLP | 0.95384 | 3.6339 | 487.2906 | 2.563 |
| MTF-GLP-HPM | 0.95633 | 3.5973 | 472.7066 | 2.5159 |
| GS | 0.92901 | 3.8802 | 603.6007 | 3.2624 |
| GSA | 0.94898 | 3.5911 | 498.8250 | 2.7418 |
| PCA | 0.91829 | 4.7033 | 657.2954 | 3.6624 |
| GFPCA | 0.89042 | 4.8472 | 745.6006 | 4.0001 |
| CNMF | 0.92986 | 4.4263 | 592.1969 | 3.1799 |
| Bayesian Naive | 0.95195 | 3.6428 | 489.5634 | 2.6286 |
| Bayesian Sparse | **0.95862** | **3.3480** | **449.4029** | **2.4767** |
| HySure | 0.94648 | 3.8648 | 511.0745 | 2.8206 |

**TABLE 5. QUALITY MEASURES FOR THE GARONS DATASET.**

| METHOD | CC | SAM | RMSE | ERGAS |
|---|---|---|---|---|
| SFIM | 0.85015 | 5.9591 | 867.6333 | 4.3969 |
| MTF-GLP | 0.86763 | 5.8218 | 796.6888 | 4.1035 |
| MTF-GLP-HPM | 0.86818 | 5.9154 | 800.0304 | 4.0758 |
| GS | 0.83384 | 5.9761 | 984.1284 | 4.8813 |
| GSA | 0.85095 | 6.1067 | 833.2378 | 4.2233 |
| PCA | 0.84693 | 5.9566 | 966.0805 | 4.8107 |
| GFPCA | 0.6339 | 7.4415 | 1312.0373 | 6.3416 |
| CNMF | 0.83038 | 6.9385 | 892.6918 | 4.4832 |
| Bayesian Naive | 0.86857 | 5.8749 | 784.1298 | 3.9147 |
| Bayesian Sparse | **0.87642** | **5.6879** | **754.9837** | **3.7776** |
| HySure | 0.86020 | 6.0658 | 780.2847 | 4.0432 |



**FIGURE 4.** RMSE between the methods' result and the reference image, per pixel for the Camargue dataset.



**FIGURE 3.** RMSE between the methods' result and the reference image, per pixel for the Moffett field dataset.
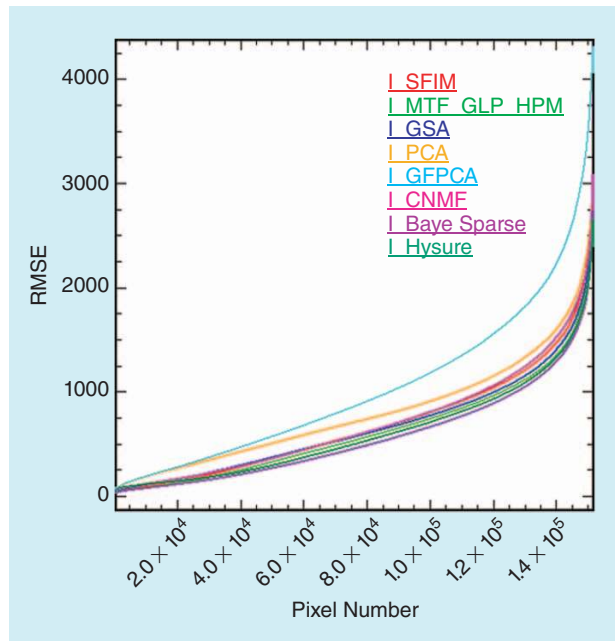


**FIGURE 5.** RMSE between the methods' result and the reference image, per pixel for the Garons dataset.

image for the three considered datasets. Note that, for sake of conciseness, some methods have not been considered here but only their improved versions are presented. More specifically, GS has been removed since GSA is an improved version of GS. Indeed, GSA is expected to give better results than GS thanks to its adaptive estimation of the weight for generating the equivalent PAN image from the HS image, which allows the spectral distortion to be reduced. Bayesian naive approach has been also removed since the sparsity-based approach relies on a more complex prior and gives also better results. MTF-GLP and MTF-GLP-HPM yield similar results so only the latter has been considered.

Figures 6 and 7 show extracts of the final result obtained by the considered methods on the Camargue dataset in the visible (R= 704.39nm, G= 557.90nm, B= 454.5nm) and in the SWIR (R= 1216.7nm, G= 1703.2nm, B= 2159.8nm) domains, respectively.

Figures 8, 9 and 10 show pixel spectra recovered by the fusion methods, which correspond to 10th, 50th and 90th percentile of RMSE, respectively. Those spectra have been selected by choosing GSA as the reference for RMSE value. GSA have been chosen since it is a classical approach that has been widely used in literature and also gives good results. To ensure a reasonable number of figures, only visual results and some spectra of the Camargue dataset has been reported in this article. The results for the two other datasets can be found in the supporting document [86] available online[5]. In
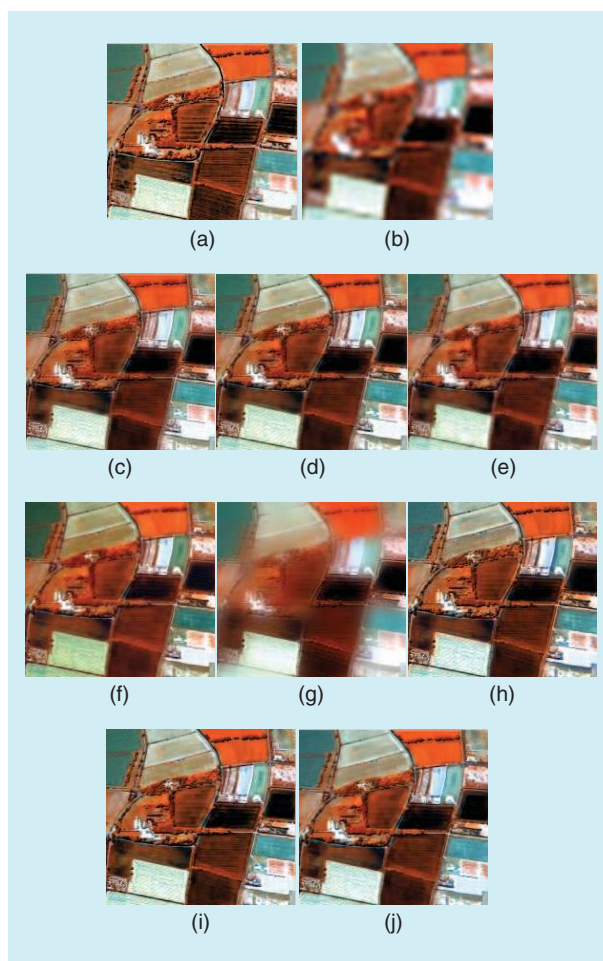
---

[5]http://openremotesensing.net
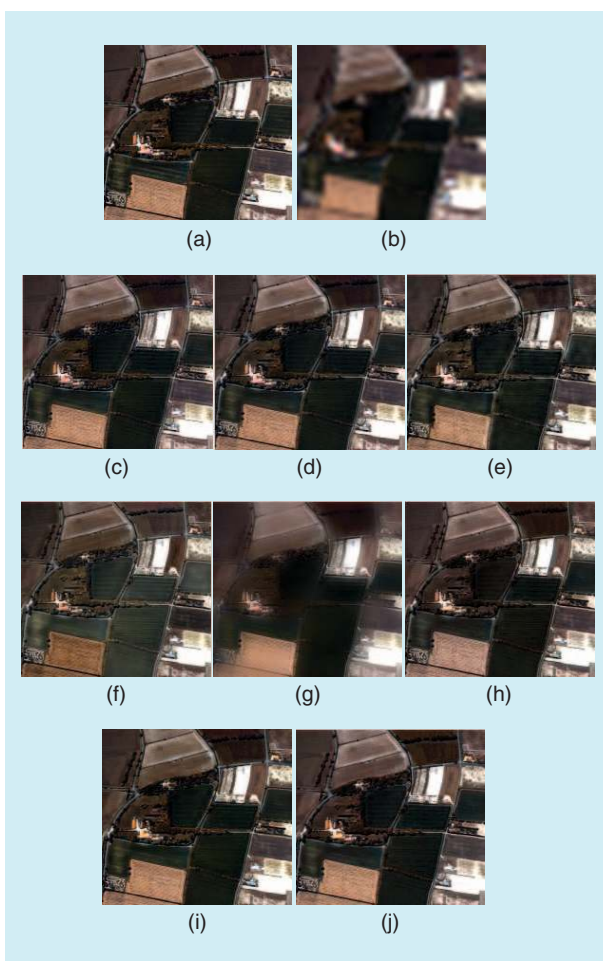
**FIGURE 6.** Details of original and fused Camargue dataset HS image in the visible domain. (a) reference image, (b) interpolated HS image, (c) SFIM, (d) MTF-GLP-HPM, (e) GSA, (f) PCA, (g) GFPCA, (h) CNMF, (i) Bayesian Sparse, (j) HySure.



**FIGURE 7.** Details of original and fused Camargue dataset HS image in the SWIR domain. (a) reference image, (b) interpolated HS image, (c) SFIM, (d) MTF-GLP-HPM, (e) GSA, (f) PCA, (g) GFPCA, (h) CNMF, (i) Bayesian Sparse, (j) HySure.

particular, because of the nature of the Garons dataset (village with a lot of small buildings) and the chosen ratio of 5, worse results have been obtained than for the two first datasets since a lot of mixing is presented in the HS image.

A visual analysis of the result shows that most of the fusion approaches considered in this paper give good results, excepted two methods: PCA and GFPCA. PCA belongs to the class of CS methods which are known to be characterized by their high fidelity in rendering the spatial details but their generation of significant spectral distortion. This is clearly visible in Figure 6 (f), where significant differences of color can be observed with respect to the reference image, in particular when examining the different fields. GFPCA here also performs poorly. Compared with PCA, there is less spectral distortion but the included spatial information seems to be not sufficient, since the fused image is significantly blurred. Spatial information provided by PCA is better since the main information of HS image (where the spatial information is contained) is replaced by the high spatial information contained in the

PAN image. When using GFPCA, the guided filter controls the amount of spatial information added to the data, so not all the spatial information may be added to avoid to modify the spectral information too much. For the Moffett field dataset, GFPCA performs a little bit better since, in this dataset, there is a lot of large areas. Thus blur is less present whereas, in the Garons dataset, GFPCA performs worse since this image consists of numerous small features, leading to more blurring effects. As a consequence, in this case, GFPCA performs worse than PCA.

To analyze the spectrum in detail, chosen thanks to RMSE percentiles, some additional information about the corresponding pixels are needed. Fig. 9 corresponds to a pixel in the reference image which represents a red building. Since in the HS image this building is mixed with its neighborhood, we do not have the same information between the reference image ("pure" spectrum) and the HS image ("mixed" spectrum). Fig. 8 corresponds to a pixel in a homogeneous field area, no mixing is present and very good results have been obtained for all the methods. For
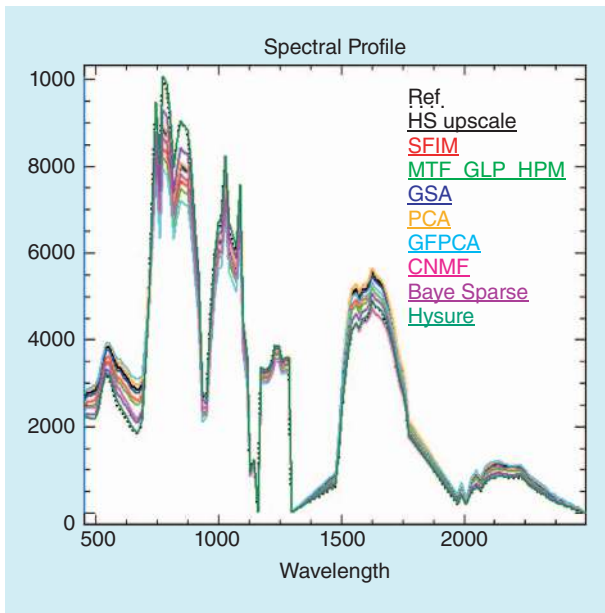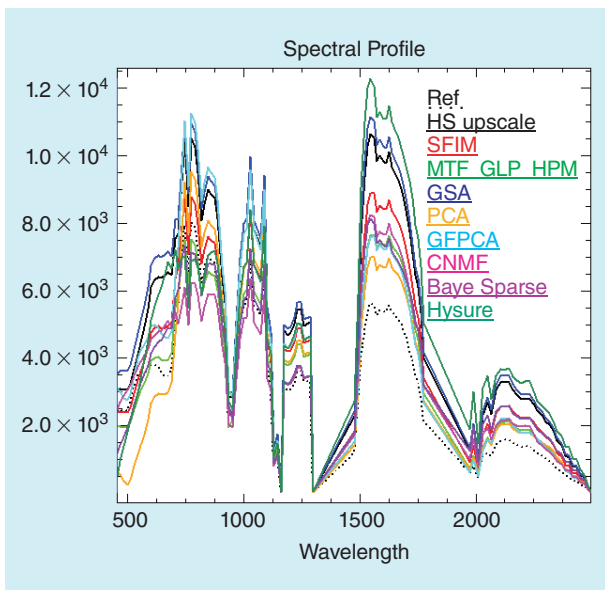
**FIGURE 8.** Luminance of the pixel corresponding to the 10th percentile of the RMSE (Camargue dataset).
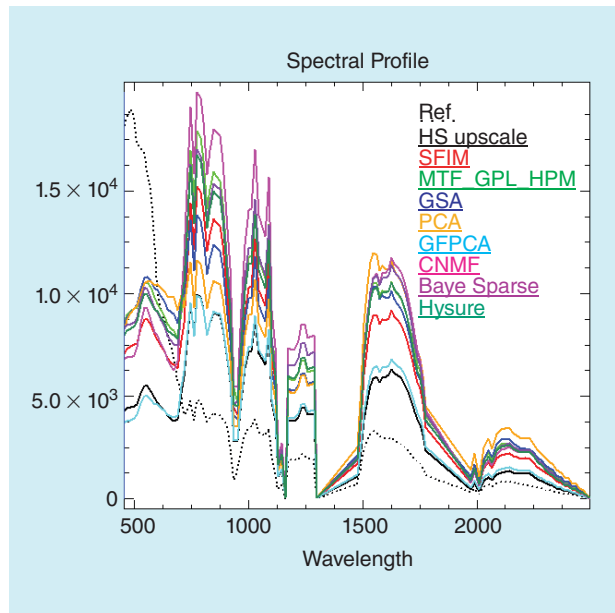


**FIGURE 10.** Luminance of the pixel corresponding to the 90th percentile of the RMSE (Camargue dataset).



**FIGURE 9.** Luminance of the pixel corresponding to the 50th percentile of the RMSE (Camargue dataset).

**TABLE 6. COMPUTATIONAL TIMES OF THE DIFFERENT METHODS (IN SECONDS).**

| METHOD | MOFFETT | CAMARGUE | GARONS |
|---|---|---|---|
| SFIM | 1.26 | 3.47 | 2.74 |
| MTF-GLP | 1.86 | 4.26 | 4.00 |
| MTF-GLP-HPM | 1.71 | 4.25 | 2.98 |
| GS | 4.77 | 8.29 | 5.56 |
| GSA | 5.52 | 8.73 | 5.99 |
| PCA | 3.46 | 8.92 | 6.09 |
| GFPCA | 2.58 | 8.51 | 4.36 |
| CNMF | 10.98 | 47.54 | 23.98 |
| Bayesian Naive | 1.31 | 7.35 | 3.07 |
| Bayesian Sparse | 133.61 | 485.13 | 259.44 |
| HySure | 140.05 | 296.27 | 177.60 |

recover spectra that are more similar to the reference spectrum than the HS spectrum.

Table 6 report the computational times required by each HS pansharpening methods on the Camargue dataset those values have been obtained with an Intel Core i5 3230M 2.6 GHz with 8 GB RAM. Based on this table, these methods can be classified as follows:

⬤ Methods which do not work well for HS pansharpening: PCA, GS, GFPCA

⬤ Methods which work well with a low time of computation (few seconds): GSA, MRA methods, Bayesian Naive

⬤ Methods which work well with an average time of computation (around one minute): CNMF

⬤ Methods which work well (slightly better) with an important time of computation (few minutes, depends greatly on the size of the dataset): Bayesian Sparse and HySure.

Fig. 10, the pixel belongs to a small white building not visible in the HS image and spectral mixing is then also present. More generally, spectra in the HS and reference images differ since some mixing processes occur in the HS image. Thus, the HS pansharpening methods are expected to provide spectra that are more similar to the HS spectra (which contains the available spectral information) than the reference (which has information missing in the HS which should not be found in the result, unless successful unmixing has been conducted). However, it is important to note that for Fig. 9, Bayesian methods and HySure successfully

To summarize, the comparison of the different methods performances for RMSE curves and quality measures confirms than PCA and GFPCA does not provide good results for HS pansharpening (GFPCA is know to perform much better on HS+RGB data). The other methods perform well, with Bayesian approaches having better results. The computational cost of Bayesian approaches depends on the chosen prior, i.e., Bayesian approach with Gaussian naive prior has low cost while the one with sparse prior has higher cost. The favorable fusion performance obtained by the Bayesian methods can be explained, in part, by the fact that they rely on a forward modeling of the PAN and HS images and explicitly exploit the spatial and spectral degradations applied to the target image. However, these algorithms may suffer from performance discrepancies when the parameters of these degradations (i.e., spatial blurring kernel, sensor spectral response) are not perfectly known. In particular, when these parameters are fully unknown and need to be fixed, they can be estimated jointly with the fused image, as in [53], or estimated from the MS and HS images in a preprocessing step, following the strategies in [78] or [35]. CS methods are fast to compute and easy to implement. They provide good spatial results but poor spectral results with significant spectral distortions, in particular when considering PCA and GS. GSA provides better results than the two other methods thanks to its adaptive weight estimation reducing the spectral distortion of the equivalent PAN image created from the HS image. MRA methods are fast, MTF-based methods give better results than SFIM and perform as well as the most competitive algorithms with higher computational complexity. SFIM does not perform as well than the other MRA methods since it uses a box filter which should give less good result. In our experimentations, results from SFIM are not so different from those obtained with the MTF-based methods. This may come from the fact that semi-synthetic datasets are used so MTF may not be fully used to its potential. Table 7 reports these pro and cons associated with each HS pansharpening method.

Finally, note that, in our experimentations, no registration error and temporal misalignment have been considered, which suggests that the robustness of the different methods has not been fully analyzed. When such problems may occur, CS and MRA methods may perform better thanks to their great robustness. In particular, CS methods are robust against misregistration error and aliasing, whereas MRA approaches are robust against aliasing and temporal misalignment. It is also worthy to note that the quality of a fusion method should also be related to a specific application (such

> FOLLOWING WALD'S PROTOCOL, THE EVALUATION INCLUDES QUALITATIVE VISUAL ASSESSMENT, AS WELL AS QUANTITATIVE EVALUATION WITH A NUMBER OF CRITERIA MEASURING SPATIAL AND SPECTRAL DISTORTIONS.

**TABLE 7. PROS AND CONS OF EACH METHOD.**

| METHOD | PROS | CONS |
|---|---|---|
| SFIM II.B.1 | 1) Low computational complexity | 1) Reduced performance when compared to MTF methods (since it uses a box filter) |
| MTF-GLP II.B.2 | 1) Performs well<br>2) Low computational complexity | |
| MTF-GLP-HPM II.B.2 | 1) Performs well<br>2) Low computational complexity | |
| GS II.A.2 | 1) Spatial information is well preserved<br>2) Low computational complexity<br>3) Easy implementation | 1) Low performance for HS images<br>2) Significant spectral distortion |
| GSA II.A.2 | 1) Spatial information is well preserved<br>2) Spectral distortion is reduced (compared to GS)<br>3) Low computational complexity<br>4) Easy implementation | |
| PCA II.A.1 | 1) Spatial information is well preserved<br>2) Low computational complexity<br>3) Easy implementation | 1) Low performance for HS images<br>2) Significant spectral distortion |
| GFPCA II.C.1 | 1) Spectral information is well preserved<br>2) Low computational complexity | 1) Low performance for HS images (work better with RGB images)<br>2) Not enough spatial information added (lot of blur) |
| CNMF II.E.1 | 1) Good results (spatial and spectral) | 1) Sensor characteristics required<br>2) Medium computational cost |
| Bayesian Naive II.D.1 | 1) Good results (spatial and spectral)<br>2) Low computational complexity | 1) Sensor characteristics required |
| Bayesian Sparse II.D.2 | 1) Good results (spatial and spectral) | 1) High computational cost<br>2) Sensor characteristics required |
| HySure II.D.3 | 1) Good results (spatial and spectral) | 1) High computational cost |

as classification or target detection). Indeed, a method providing images with good performance metrics may or may not be the best for this specific application.

## V. CONCLUSION

In this paper a qualitative and quantitative comparison of 11 different HS pansharpening methods was conducted, considering classical MS pansharpening techniques adapted to the HS context, and methods originally designed for HS pansharpening. More precisely, five classes of methods were presented: CS, MRA, Hybrid, Bayesian and matrix factorization. Those methods were evaluated on three different datasets representative of various scenario: mixed urban/rural area, rural area and urban area.

A careful analysis of their performances suggested a classification of these methods into four groups: i) Methods with poor fusion results (CS-based methods (GS and PCA) and GFPCA), ii) Methods with good fusion performances and low computational costs (MRA methods, GSA and Bayesian naive) that may be suitable for fusing large scale images, which is often the case for spaceborne hyperspectral imaging missions, iii) Methods with good fusion performances and reasonable computational costs (CNMF), iv) Methods with slightly better fusion results but with higher computational costs (HySure and Bayesian Sparse). Those results were obtained with semi-synthetic datasets with no registration error or temporal misalignment. Thus robustness of the methods against these issues were not taken into account. When such problems may happen, different results could be obtained and classical pansharpening methods (CS and MRA) may give better results thanks to their robustness to these specific issues.

The experiments and the quality measures presented in this paper were performed using MATLAB implementations of the algorithms. A MATLAB toolbox is made available online[6] to the community to help improve and develop new HS pansharpening methods and to facilitate comparison of the different methods.

## VI. ACKNOWLEDGMENT

> **WHILE METHODS DERIVED FROM STANDARD PANSHARPENING (PAN+MS) PROVIDE SOUND STRATEGIES, HYPERSPECTRAL PANSHARPENING (PAN+HS) STILL OFFERS NEW AVENUES OF SPECIFIC RESEARCH.**

## AUTHOR INFORMATION

**Laetitia Loncan**, *received the engineer degree in Electrical engineering from the Grenoble Institute of Technology (Grenoble, France) in 2013. She is currently a second year Ph.D. student working with ONERA (Toulouse, France) and GIPSA-LAB (Grenoble, France). Her research activities are focused around data fusion in remote sensing, particularly Pansharpening.*

**Luís B. Almeida** *received the "Doutor" degree from the Technical University of Lisbon in 1983. Since 1972, he has been a faculty member of Instituto Superior Técnico (IST), Lisbon University, where he has been a full professor since 1995, in the areas of signal processing and machine learning. From 1984 to 2004, he was head of the Neural Networks and Signal Processing Group of INESC-ID. From 2000 to 2003, he was chair of INESC-ID. In 2005, he joined the Instituto de Telecomunicações (Telecommunications Institute). From 2008 to 2010, he was chair of the Electrical and Computer Engineering Department of IST. Over the years, he has worked on speech modeling and coding, time-frequency representations of signals and the fractional Fourier transform, learning algorithms for neural networks, blind source separation, and, currently, image processing. He was the recipient of an IEEE Signal Processing Area ASSP Senior Award and of several national awards.*

**José M. Bioucas-Dias** *(S'87, M'95) received the EE, MSc, PhD, and "Agregado" degrees from Instituto Superior Técnico (IST), Technical University of Lisbon (TULisbon, now University of Lisbon), Portugal, in 1985, 1991, 1995, and 2007, respectively, all in electrical and computer engineering. Since 1995, he has been with the Department of Electrical and Computer Engineering, IST, where he was an Assistant Professor from 1995 to 2007 and an Associate Professor since 2007. Since 1993, he is also a Senior Researcher with the Pattern and Image Analysis group of*

the Instituto de Telecomunicações, which is a private non-profit research institution. His research interests include inverse problems, signal and image processing, pattern recognition, optimization, and remote sensing. Dr. Bioucas-Dias has authored or co-authored more than 250 scientific publications including more than 70 journal papers (48 of which published in IEEE journals) and 180 peer-reviewed international conference papers and book chapters. Dr. Bioucas-Dias was an Associate Editor for the IEEE Transactions on Circuits and Systems (1997–2000) and he is an Associate Editor for the IEEE Transactions on Image Processing and IEEE Transactions on Geoscience and Remote Sensing. He was a Guest Editor of IEEE Transactions on Geoscience and Remote Sensing for the Special Issue on Spectral Unmixing of Remotely Sensed Data, of IEEE Journal of Selected Topics in Applied Earth Observations and Remote Sensing for the Special Issue on Hyperspectral Image and Signal Processing, of IEEE Signal Processing Magazine for the Special Issue on Signal and Image Processing in Hyperspectral Remote Sensing, of IEEE Journal of Selected Topics in Signal Processing for the Advances in Hyperspectral Data Processing and Analysis, and of IEEE Geoscience and Remote Sensing Magazine for the Special Issue on Advances in Machine Learning for Remote Sensing and Geosciences. He was the General Co-Chair of the 3rd IEEE GRSS Workshop on Hyperspectral Image and Signal Processing, Evolution in Remote sensing (WHISPERS'2011) and has been a member of program/technical committees of several international conferences.

**Xavier Briottet** received his PhD degree in Electonics from the Ecole Nationale Supérieure de l'Aéronautique et de l'Espace (Toulouse, France) in 1986 and his "Habilitation Diriger les Recherches" in 1999 from Paul Sabatier University. In 1987, he became an assistant professor in signal and image processing at the Ecole Supérieure d'Électricité. He is now Director of Research and the advisor of the scientific politic at DOTA. Since 1988, he is working in remote sensing at ONERA in the optic department (Toulouse, France). His current research interests are on 3D radiative transfer in urban area, shadow detection, atmosphere, unmixing in the reflective and thermal domain, using high spatial hyperspectral imagery and lidar.

**Jocelyn Chanussot** (M'04-SM'04-F'12) received the M.Sc. degree in electrical engineering from the Grenoble Institute of Technology (Grenoble INP), Grenoble, France, in 1995, and the Ph.D. degree from Savoie University, Annecy, France, in 1998. In 1999, he was with the Geography Imagery Perception Laboratory for the Delegation Generale de l'Armement (DGA-French National Defense Department). Since 1999, he has been with Grenoble INP, where he was an Assistant Professor from 1999 to 2005, an Associate Professor from 2005 to 2007, and is currently a Professor of signal and image processing. He is conducting his research at the Grenoble Images Speech Signals and Automatics Laboratory (GIPSA-Lab). His research interests include image analysis, multicomponent image processing, nonlinear filtering, and data fusion in remote sensing. He is a member of the Institut Universitaire de France (2012-2017). Since 2013, he is an Adjunct Professor of the University of Iceland. Dr. Chanussot is the founding President of IEEE Geoscience and Remote Sensing French chapter (2007-2010) which received the 2010 IEEE GRS-S Chapter Excellence Award. He was the co-recipient of the NORSIG 2006 Best Student Paper Award, the IEEE GRSS 2011 Symposium Best Paper Award, the IEEE GRSS 2012 Transactions Prize Paper Award and the IEEE GRSS 2013 Highest Impact Paper Award. He was a member of the IEEE Geoscience and Remote Sensing Society AdCom (2009-2010), in charge of membership development. He was the General Chair of the first IEEE GRSS Workshop on Hyperspectral Image and Signal Processing, Evolution in Remote sensing (WHISPERS). He was the Chair (2009-2011) and Cochair of the GRS Data Fusion Technical Committee (2005-2008). He was a member of the Machine Learning for Signal Processing Technical Committee of the IEEE Signal Processing Society (2006-2008) and the Program Chair of the IEEE International Workshop on Machine Learning for Signal Processing, (2009). He was an Associate Editor for the IEEE Geoscience and Remote Sensing Letters (2005-2007) and for Pattern Recognition (2006-2008). Since 2007, he is an Associate Editor for the IEEE Transactions on Geoscience and Remote Sensing. Since 2011, he is the Editor-in-Chief of the IEEE Journal of Selected Topics in Applied Earth Observations and Remote Sensing. In 2013, he was a Guest Editor for the Proceedings of the IEEE and in 2014 a Guest Editor for the IEEE Signal Processing Magazine. He is a Fellow of the IEEE and a member of the Institut Universitaire de France (2012-2017).

**Nicolas Dobigeon** (S'05-M'08-SM'13) was born in Angoulême, France, in 1981. He received the Eng. degree in Electrical Engineering from ENSEEIHT, Toulouse, France, and the M.Sc. degree in Signal Processing from the National Polytechnic Institute of Toulouse (INP Toulouse), both in 2004. He received the Ph.D. degree and the Habilitation à Diriger des Recherches in Signal Processing from the INP Toulouse in 2007 and 2012, respectively. From 2007 to 2008, he was a Postdoctoral Research Associate with the Department of Electrical Engineering and Computer Science, University of Michigan, Ann Arbor. Since 2008, Nicolas Dobigeon has been with the National Polytechnic Institute of Toulouse (INP-ENSEEIHT, University of Toulouse) where he is currently an Associate Professor. He conducts his research within the Signal and Communications Group of the IRIT Laboratory and he is also an affiliated faculty member of the Telecommunications for Space and Aeronautics (TeSA) cooperative laboratory. His recent research activities have been focused on statistical signal and image processing, with a particular interest in Bayesian inverse problems with applications to remote sensing, biomedical imaging and genomics.

**Sophie Fabre**, *research engineer, received the post graduate in Signal and Image Processing (UPS, Toulouse III, and France) in 1996 and the doctorate of signal, image and communication (ISAE, Toulouse, France) in 1999 on multi-sensor fusion. She worked during five year on projects FARM-STAR (precision crop management) and GEOLAND (European project on the vegetation characterization using multi-temporal MERIS data) on behalf of ASTRIUM (France). Then, she joined THALES Services (France) during one year to support the specification of the PLEIADES radiometric correction module. Finally, she joined the department DOTA (Theorectical and Applied Optics Department) part of Onera since 2006 in order to work on hyperspectral data processing. She is providing since 2007 the project STAD, ground segment of the Sysiphe system (airborne hyperspectral instruments covering the spectral domain [0.4–12 m] at a spatial resolution of 0.5 m) for DGA (France). Its recent works first concern the geometric correction, the inter-instrument registration in the STAD frame and on the other hand the estimation of physical parameters (soil moisture content ) owing to hyperspectral data processing.*

**Wenzhi Liao** *(S'10-M'14) received the B.S. degree in mathematics from Hainan Normal University, HaiKou, China, in 2006, the Ph.D. degree in engineering from South China University of Technology, Guangzhou, China, in 2012, and the Ph.D. degree in computer science engineering from Ghent University, Ghent, Belgium, in 2012. Since 2012, he has been working as a Postdoc with Ghent University. His research interests include pattern recognition, remote sensing, and image processing, in particular, hyperspectral image restoration, mathematical morphology, data fusion, and classification. Dr. Liao is a member of the Geoscience and Remote Sensing Society (GRSS) and the IEEE GRSS Data Fusion Technical Committee (DFTC). He was the recipient of the "Best Paper Challenge" Awards on both 2013 IEEE GRSS Data Fusion Contest and 2014 IEEE GRSS Data Fusion Contest.*

**Giorgio A. Licciardi** *received the M.S. degree in telecommunication engineering and the Ph.D. degree in geoinformation from the Tor Vergata University, Rome, Italy, in 2005 and 2010, respectively. In 2010 he joined the Laboratoire Grenoblois de l'Image, de la Parole, du Signal et de l'Automatique (GIPSA-Lab) as a Postdoctoral Fellow. His main research is focused on hyperspectral image processing, including feature extraction techniques, spectral unmixing, super-resolution and Pansharpening. From 2014 he is Ingnieur de recherch at the Grenoble Institute of Technology. He is also a European Space Agency Category-1 Principal Investigator for Earth observation data. Dr. Licciardi serves as a Referee for several scientific journals such as the IEEE Transactions on Geoscience and Remote Sensing the IEEE Geoscience and Remote Sensing Letters and*

*IEEE Journal of Selected Topics in Applied Earth Observations and Remote Sensing.*

**Miguel Simões** *was born in Lisbon, Portugal, in 1987. He received the M.Sc. degree in electrical and computer engineering from the Instituto Superior Técnico, University of Lisbon, Lisbon, in 2010. He is currently working toward the joint Ph.D. degree in electrical and computer engineering, and signal and image processing at the Instituto de Telecomunicações, Instituto Superior Técnico, University of Lisbon, Lisbon, and at the Grenoble Images Parole Signal Automatique (GIPSA-lab), University of Grenoble, Grenoble, France, respectively. Previously, he has worked as an Information Technology (IT) consultant in the field of telecommunications. His main areas of research interest are image processing, optimization, and remote sensing.*

**Jean-Yves Tourneret** *(SM'08) received the ingnieur degree in electrical engineering from the École nationale supérieure d'électrotechnique, d'électronique, d'informatique, d'hydraulique et des télécommunications (ENSEEIHT) de Toulouse in 1989 and the Ph.D. degree from the National Polytechnic Institute from Toulouse in 1992. He is currently a professor in the university of Toulouse (ENSEEIHT) and a member of the IRIT laboratory (UMR 5505 of the CNRS). His research activities are centered around statistical signal and image processing with a particular interest to Bayesian and Markov chain Monte Carlo (MCMC) methods. He has been involved in the organization of several conferences including the European conference on signal processing EUSIPCO'02 (program chair), the international conference ICASSP06 (plenaries), the statistical signal processing workshop SSP12 (international liaisons), the International Workshop on Computational Advances in Multi-Sensor Adaptive Processing CAMSAP 2013 (local arrangements), the statistical signal processing workshop SSP'2014 (special sessions), the workshop on machine learning for signal processing MLSP2014 (special sessions). He has been the general chair of the CIMI workshop on optimization and statistics in image processing hold in Toulouse in 2013 (with F. Malgouyres and D. Kouamé) and of the International Workshop on Computational Advances in Multi-Sensor Adaptive Processing CAMSAP 2015 (with P. Djuric). He has been a member of different technical committees including the Signal Processing Theory and Methods (SPTM) committee of the IEEE Signal Processing Society (2001-2007, 2010-present). He has been serving as an associate editor for the IEEE Transactions on Signal Processing (2008-2011) and for the EURASIP journal on Signal Processing (since July 2013).*

**Miguel A. Veganzones** *(M'12) received the M.Sc. and Ph.D. degrees in computer science from the Basque Country University (UPV/EHU), Donostia, Spain, in 2005 and 2012 respectively. Since 2012, he is a posdoctoral researcher at the Images-Signal*

department in the GIPSA-lab, Grenoble, France. His current main research activities focus in the analysis of hyperspectral images by means of computational intelligence and statistical techniques. Currently he is a research member of the ERC FP7/2007-2013 Grant Agreement no. 320594 DECODA project. He has served as a scientific reviewer in several IEEE publications.

**Gemine Vivone** received the B.Sc. (cum laude), the M.Sc. (cum laude), and the Ph.D. degrees in information engineering from the University of Salerno, Salerno, Italy, in 2008, 2011, and 2014, respectively. He is currently a Scientist at the North Atlantic Treaty Organization (NATO) Science & Technology Organization (STO) Centre for Maritime Research and Experimentation (CMRE), La Spezia, Italy. In 2014, he joined the NATO STO CMRE, La Spezia, Italy as a Research Fellow. In 2013, he was as a Visiting Scholar with Grenoble Institute of Technology (INPG), Grenoble, France, conducting his research at the Laboratoire Grenoblois de l'Image, de la Parole, du Signal et de l'Automatique GIPSA-Lab. In 2012, he was a Visiting Researcher with the NATO Undersea Research Centre, La Spezia, Italy. His main research interests focus on statistical signal processing, detection of remotely sensed images, data fusion, and tracking algorithms. Dr. Vivone serves as a Referee for IEEE Transactions on Geoscience and Remote Sensing, IEEE Journal of Selected Topics in Applied Earth Observations and Remote Sensing, and IEEE Geoscience and Remote Sensing Letters. Dr. Vivone was the recipient of the Symposium Best Paper Award at the IEEE International Geoscience and Remote Sensing Symposium (IGARSS) 2015.

**Qi Wei** (S'13) was born in Shanxi, China, in 1989. He received the B.Sc degree in electrical engineering from Beihang University (BUAA), Beijing, China in 2010. From February to August of 2012, he was an exchange master student with the Signal Processing and Communications Group at the Department of Signal Theory and Communications (TSC), Universitat Politècnica de Catalunya (UPC). Since September of 2012, he has been a PhD student with the National Polytechnic Institute of Toulouse (University of Toulouse, INP-ENSEEIHT). He is also with the Signal and Communications Group of the IRIT Laboratory. His research has been focused on statistical signal processing, especially on inverse problems in image processing.

**Naoto Yokoya** (S'10-M'13) received the M.Sc. and Ph.D. degrees in aerospace engineering from the University of Tokyo, Tokyo, Japan, in 2010 and 2013, respectively. He was a Research Fellow with the Japan Society for the Promotion of Science from 2012 to 2013. He is currently an Assistant Professor with the University of Tokyo. His current research interests include image analysis and data fusion in remote sensing.

## REFERENCES

[1] [Online]. Available: http://smsc.cnes.fr/PLEIADES/index.htm

[2] S. Michel, P. Gamet, and M.-J. Lefevre-Fonollosa, "HYPXIM—A hyperspectral satellite defined for science, security and defence users," in *Proc. 3rd Workshop Hyperspectral Image Signal Processing: Evolution in Remote Sensing*), Lisbon, Portugal, June 2011, pp. 1–4.

[3] L. Alparone, L. Wald, J. Chanussot, C. Thomas, P. Gamba, and L. M. Bruce, "Comparison of pansharpening algorithms: Outcome of the 2006 GRS-S data-fusion contest," *IEEE Trans. Geosci. Remote Sensing*, vol. 45, no. 10, pp. 3012–3021, Oct. 2007.

[4] G. Vivone, L. Alparone, J. Chanussot, M. D. Mura, Garzelli, and G. Licciardi, "A critical comparison of pansharpening algorithms," in *Proc. IEEE Int. Conf. Geoscience Remote Sensing*, July 2014, pp. 191–194.

[5] B. Aiazzi, L. Alparone, S. Baronti, A. Garzelli, and M. Selva, "25 years of pansharpening: A critical review and new developments," in *Signal Image Processing for Remote Sensing*, 2nd ed., C. H. Chen, Ed. Boca Raton, FL: CRC Press, 2011, ch. 28, pp. 533–548.

[6] C. Thomas, T. Ranchin, L. Wald, and J. Chanussot, "Synthesis of multispectral images to high spatial resolution: A critical review of fusion methods based on remote sensing physics," *IEEE Trans. Geosci. Remote Sensing*, vol. 46, no. 5, pp. 1301–1312, May 2008.

[7] W. Carper, T. M. Lillesand, and P. W. Kiefer, "The use of Intensity-Hue-Saturation transformations for merging SPOT panchromatic and multispectral image data," *Photogramm. Eng. Remote Sens.*, vol. 56, no. 4, pp. 459–467, Apr. 1990.

[8] T.-M. Tu, S.-C. Su, H.-C. Shyu, and P. S. Huang, "A new look at IHS-like image fusion methods," *Inform. Fusion*, vol. 2, no. 3, pp. 117–186, Sept. 2001.

[9] P. S. Chavez, Jr., S. C. Sides, and J. A. Anderson, "Comparison of three different methods to merge multiresolution and multispectral data: Landsat TM and SPOT panchromatic," *Photogramm. Eng. Remote Sens.*, vol. 57, no. 3, pp. 295–303, Mar. 1991.

[10] P. S. Chavez and A. Y. Kwarteng, "Extracting spectral contrast in Landsat thematic mapper image data using selective principal component analysis," *Photogramm. Eng. Remote Sens.*, vol. 55, no. 3, pp. 339–348, 1989.

[11] V. Shettigara, "A generalized component substitution technique for spatial enhancement of multispectral images using a higher resolution data set," *Photogramm. Eng. Remote Sens.*, vol. 58, no. 5, pp. 561–567, 1992.

[12] V. P. Shah, N. Younan, and R. L. King, "An efficient pan-sharpening method via a combined adaptive PCA approach and contourlets," *IEEE Trans. Geosci. Remote Sensing*, vol. 56, no. 5, pp. 1323–1335, May 2008.

[13] C. Laben and B. Brower, "Process for enhacing the spatial resolution of multispectral imagery using pan-sharpening," U.S. Patent 6 011 875, Jan. 4, 2000.

[14] S. Mallat, "A theory for multiresolution signal decomposition: The wavelet representation," *IEEE Trans. Pattern Anal. Mach. Intell.*, vol. 11, no. 7, pp. 674–693, July 1989.

[15] G. P. Nason and B. W. Silverman, "The stationary wavelet transform and some statistical applications," in *Wavelets and Statistics*, vol. 103, A. Antoniadis and G. Oppenheim, Eds. New York: Springer-Verlag, 1995, pp. 281–299.

[16] M. J. Shensa, "The discrete wavelet transform: Wedding the a trous and Mallat algorithms," *IEEE Trans. Signal Processing*, vol. 40, no. 10, pp. 2464–2482, Oct. 1992.

[17] P. J. Burt and E. H. Adelson, "The Laplacian pyramid as a compact image code," *IEEE Trans. Commun.*, vol. 31, no. 4, pp. 532–540, Apr. 1983.

[18] M. N. Do and M. Vetterli, "The contourlet transform: An efficient directional multiresolution image representation," *IEEE Trans. Image Processing*, vol. 14, no. 12, pp. 2091–2106, Dec. 2005.

[19] J. F. J.-L. Starck and F. Murtagh, "The undecimated wavelet decomposition and its reconstruction," *IEEE Trans. Image Processing*, vol. 16, no. 2, pp. 297–309, Feb. 2007.

[20] C. Ballester, V. Caselles, L. Igual, J. Verdera, and B. Rougé, "A variational model for P+XS image fusion," *Int. J. Comput. Vis.*, vol. 5969, no. 1, pp. 43–58, 2006.

[21] F. Palsson, J. Sveinsson, M. Ulfarsson, and J. A. Benediktsson, "A new pansharpening algorithm based on total variation," *IEEE Geosci. Remote Sensing Lett.*, vol. 11, no. 1, pp. 318–322, Jan. 2013.

[22] X. He, L. Condat, J. B. Dias, J. Chanussot, and J. Xia, "A new pansharpening method based on spatial and spectral sparsity priors," *IEEE Trans. Image Processing*, vol. 23, no. 9, pp. 4160–4174, Sept. 2014.

[23] M. Moeller, T. Wittman, and A. L. Bertozzi, "A variational approach to hyperspectral image fusion," in *Proc. SPIE Defense, Security, Sensing*, 2009.

[24] A. Garzelli, B. Aiazzi, S. Baronti, M. Selva, and L. Alparone, "Hyperspectral image fusion," in *Proc. Hyperspectral Workshop*, 2010, pp. 17–19.

[25] L. Alparone, B. Aiazzi, S. Baronti, and A. Garzelli, *Remote Sensing Image Fusion* (Signal and Image Processing of Earth Observations). Boca Raton, FL: CRC Press, 2015.

[26] G. Vivone, L. Alparone, J. Chanussot, M. D. Mura, A. Garzelli, and G. Licciardi, "MultiResolution analysis and component substitution techniques for hyperspectral Pansharpening," in *Proc. IEEE Int. Geoscience Remote Sensing Symp.*, July 2014, pp. 2649–2652.

[27] J. M. B. Dias, A. Plaza, N. Dobigeon, M. Parente, Q. Du, P. Gader, and J. Chanussot, "Hyperspectral unmixing overview: Geometrical, statistical, and sparse regression-based approaches," *IEEE J. Select. Topics Appl. Earth Observ. Remote Sensing*, vol. 5, no. 2, pp. 354–379, Apr. 2012.

[28] C. Souza, Jr, L. Firestone, L. M. Silva, and D. Roberts, "Mapping forest degradation in the Eastern amazon from SPOT 4 through spectral mixture models," *Remote Sens. Environ.*, vol. 87, no. 4, pp. 494–506, 2003.

[29] A. Mohammadzadeh, A. Tavakoli, and M. J. V. Zoej, "Road extraction based on fuzzy logic and mathematical morphology from pansharpened IKONOS images," *Photogramm. Rec.*, vol. 21, no. 113, pp. 44–60, Feb. 2006.

[30] F. Laporterie-Déjean, H. de Boissezon, G. Flouzat, and M.-J. Lefévre-Fonollosa, "Thematic and statistical evaluations of five panchromatic/multispectral fusion methods on simulated PLEIADES-HR images," *Inform. Fusion*, vol. 6, pp. 193–212, 2005.

[31] G. A. Licciardi, A. Villa, M. M. Khan, and J. Chanussot, "Image fusion and spectral unmixing of hyperspectral images for spatial improvement of classification maps," in *Proc. IEEE Int. Conf. Geoscience Remote Sensing*, 2012, pp. 7290–729.

[32] N. Yokoya, T. Yairi, and A. Iwasaki, "Coupled nonnegative matrix factorization unmixing for hyperspectral and multispectral data fusion," *IEEE Trans. Geosci. Remote Sensing*, vol. 50, no. 2, pp. 528–537, Feb. 2012.

[33] Q. Wei, N. Dobigeon, and J.-Y. Tourneret, "Bayesian fusion of multi-band images," *IEEE J. Select. Topics Signal Processing*, vol. 9, no. 6, pp. 1117–1127, Sept. 2015.

[34] Q. Wei, N. Dobigeon, and J.-Y. Tourneret, "Bayesian fusion of hyperspectral and multispectral images," in *Proc. IEEE Int. Conf. Acoust., Speech, Signal Processing*, Florence, Italy, May 2014, pp. 3176–3180.

[35] M. Simões, J. B. Dias, L. Almeida, and J. Chanussot, "A convex formulation for hyperspectral image superresolution via subspace-based regularization," *IEEE Trans. Geosci. Remote Sensing*, 2015, to be published.

[36] Q. Wei, J. M. B. Dias, N. Dobigeon, and J.-Y. Tourneret, "Hyperspectral and multispectral image fusion based on a sparse representation," *IEEE Trans. Geosci. Remote Sensing*, vol. 53, no. 7, pp. 3658–3668, Sept. 2015.

[37] B. Aiazzi, S. Baronti, and M. Selva, "Improving component substitution pansharpening through multivariate regression of MS+pan data," *IEEE Trans. Geosci. Remote Sensing*, vol. 45, no. 10, pp. 3230–3239, Oct. 2007.

[38] S. Baronti, B. Aiazzi, M. Selva, A. Garzelli, and L. Alparone, "A theoretical analysis of the effects of aliasing and misregistration on pansharpened imagery," *IEEE J. Select. Topics Signal Processing*, vol. 5, no. 3, pp. 446–453, June 2011.

[39] G. Vivone, L. Alparone, J. Chanussot, M. D. Mura, A. Garzelli, and G. Licciardi, "A critical comparison among pansharpening algorithms," *IEEE Trans. Geosci. Remote Sensing*, vol. 53, no. 5, pp. 2565–2586, May 2015.

[40] T.-M. Tu, P. S. Huang, C.-L. Hung, and C.-P. Chang, "A fast intensity-hue-saturation fusion technique with spectral adjustment for IKONOS imagery," *IEEE Trans. Geosci. Remote Sensing Lett.*, vol. 1, no. 4, pp. 309–312, 2004.

[41] B. Aiazzi, S. Baronti, F. Lotti, and M. Selva, "A comparison between global and context-adaptive pansharpening of multispectral images," *IEEE Trans. Geosci. Remote Sensing Lett.*, vol. 6, no. 2, pp. 302–306, Apr. 2009.

[42] G. Vivone, R. Restaino, M. D. Mura, G. Licciardi, and J. Chanussot, "Contrast and error-based fusion schemes for multispectral image pansharpening," *IEEE Trans. Geosci. Remote Sensing Lett.*, vol. 11, no. 5, pp. 930–934, May 2014.

[43] J. G. Liu, "Smoothing filter based intensity modulation: A spectral preserve image fusion technique for improving spatial details," *Int. J. Remote Sens.*, vol. 21, no. 18, pp. 3461–3472, Dec. 2000.

[44] L. Alparone, B. Aiazzi, S. Baronti, and A. Garzelli, "Sharpening of very high resolution images with spectral distortion minimization," in *Proc. IEEE Int. Conf. Geoscience Remote Sensing*, July 2003, pp. 458–460.

[45] B. Aiazzi, L. Alparone, S. Baronti, A. Garzelli, and M. Selva, "MTF-tailored multiscale fusion of high-resolution MS and pan imagery," *Photogramm. Eng. Remote Sens.*, vol. 72, no. 5, pp. 591–596, May 2006.

[46] K. He, J. Sun, and X. Tang, "Guided image filtering," *IEEE Trans. Pattern Anal. Mach. Intell.*, vol. 35, no. 6, pp. 1397–1409, 2013.

[47] X. Kang, J. Li, and J. A. Benediktsson, "Spectral–spatial hyperspectral image classification with edge-preserving filtering," *IEEE Trans. Geosci. Remote Sensing*, vol. 52, no. 5, pp. 2666–2677, 2014.

[48] W. Liao, X. Huang, F. Coillie, S. Gautama, A. Pizurica, W. Philips, H. Liu, T. Zhu, M. Shimoni, G. Moser, and D. Tuia, "Processing of multiresolution thermal hyperspectral and digital color data: Outcome of the 2014 IEEE GRSS data fusion contest," *IEEE J. Select. Top. Appl. Earth Observ. Remote Sensing*, vol. 8, no. 6, pp. 2984–2996, May 2015.

[49] W. Liao, B. Goossens, J. Aelterman, H. Luong, A. Pizurica, N. Wouters, W. Saeys, and W. Philips, "Hyperspectral image deblurring with PCA and total variation," in *Proc. IEEE GRSS Workshop Hyperspectral Image Signal Process.: Evolution Remote Sensing*, Florida, June 2013, pp. 1–4.

[50] R. C. Hardie, M. T. Eismann, and G. L. Wilson, "MAP estimation for hyperspectral image resolution enhancement using an auxiliary sensor," *IEEE Trans. Image Processing*, vol. 13, no. 9, pp. 1174–1184, Sept. 2004.

[51] Y. Zhang, S. de Backer, and P. Scheunders, "Noise-resistant wavelet-based Bayesian fusion of multispectral and hyperspectral images," *IEEE Trans. Geosci. Remote Sensing*, vol. 47, no. 11, pp. 3834–3843, Nov. 2009.

[52] M. Joshi and A. Jalobeanu, "MAP estimation for multiresolution fusion in remotely sensed images using an IGMRF prior model," *IEEE Trans. Geosci. Remote Sensing*, vol. 48, no. 3, pp. 1245–1255, Mar. 2010.

[53] Q. Wei, N. Dobigeon, and J.-Y. Tourneret, "Bayesian fusion of multispectral and hyperspectral images with unknown sensor spectral response," in *Proc. IEEE Int. Conf. Image Processing*, Paris, France, Oct. 2014, pp. 698–702.

[54] M. Simões, J. B. Dias, L. B. Almeida, and J. Chanussot, "Hyperspectral image superresolution: An edge-preserving convex formulation," in *Proc. IEEE Int. Conf. Image Processing*, Paris, France, Oct. 2014, pp. 4166–4170.

[55] R. Molina, A. K. Katsaggelos, and J. Mateos, "Bayesian and regularization methods for hyperparameter estimation in image restoration," *IEEE Trans. Image Processing*, vol. 8, no. 2, pp. 231–246, 1999.

[56] R. Molina, M. Vega, J. Mateos, and A. K. Katsaggelos, "Variational posterior distribution approximation in Bayesian super resolution reconstruction of multispectral images," *Appl. Comput. Harmon. Anal.*, vol. 24, no. 2, pp. 251–267, 2008.

[57] A. K. Gupta and D. K. Nagar, *Matrix Variate Distributions* (Monographs and surveys in pure and applied mathematics, vol. 104). Boca Raton, FL: Chapman & Hall/CRC, 2000.

[58] M. D. Farrell, Jr and R. M. Mersereau, "On the impact of PCA dimension reduction for hyperspectral detection of difficult targets," *IEEE Geosci. Remote Sensing Lett.*, vol. 2, no. 2, pp. 192–195, 2005.

[59] J. M. Nascimento and J. M. B. Dias, "Vertex component analysis: A fast algorithm to unmix hyperspectral data," *IEEE Trans. Geosci. Remote Sensing*, vol. 43, no. 4, pp. 898–910, Apr. 2005.

[60] Q. Wei, N. Dobigeon, and J.-Y. Tourneret, "Bayesian fusion of multispectral and hyperspectral images using a block coordinate descent method," in *Proc. IEEE GRSS Workshop Hyperspectral Image Signal Processing: Evolution Remote Sensing*, Tokyo, Japan, June 2015.

[61] Q. Wei, N. Dobigeon, and J.-Y. Tourneret, "Fast fusion of multiband images based on solving a sylvester equation," *IEEE Trans. Image Processing*, vol. 24, no. 11, pp. 4109–4121, Nov. 2015.

[62] S. Mallat, *A Wavelet Tour of Signal Processing*. New York: Academic Press, 1999.

[63] J.-L. Starck, E. Candes, and D. Donoho, "The curvelet transform for image denoising," *IEEE Trans. Image Processing*, vol. 11, no. 6, pp. 670–684, 2002.

[64] N. Ahmed, T. Natarajan, and K. Rao, "Discrete cosine transform," *IEEE Trans. Comput.*, vol. C-23, no. 1, pp. 90–93, 1974.

[65] M. Elad and M. Aharon, "Image denoising via sparse and redundant representations over learned dictionaries," *IEEE Trans. Image Processing*, vol. 15, no. 12, pp. 3736–3745, 2006.

[66] O. G. Guleryuz, "Nonlinear approximation based image recovery using adaptive sparse reconstructions and iterated denoising—Part I: Theory," *IEEE Trans. Image Processing*, vol. 15, no. 3, pp. 539–554, 2006.

[67] A. Gelman, J. B. Carlin, H. S. Stern, D. B. Dunson, A. Vehtari, and D. B. Rubin, *Bayesian Data Analysis*. 3rd ed. Boca Raton, FL: CRC Press, 2013.

[68] X. Bresson and T. Chan, "Fast dual minimization of the vectorial total variation norm and applications to color image processing," *Inverse Problems Image*, vol. 2, no. 4, pp. 455–484, 2008.

[69] M. Afonso, J. B. Dias, and M. Figueiredo, "An augmented lagrangian approach to the constrained optimization formulation of imaging inverse problems," *IEEE Trans. Image Processing*, vol. 20, no. 3, pp. 681–695, 2011.

[70] O. Berné, A. Tielens, P. Pilleri, and C. Joblin, "Non-negative matrix factorization pansharpening of hyperspectral data: An application to mid-infrared astronomy," in *Proc. IEEE GRSS Workshop Hyperspectral Image Signal Process.: Evolution Remote Sensing*, 2010, pp. 1–4.

[71] R. Kawakami, J. Wright, Y. Tai, Y. Matsushita, M. Ben-Ezra, and K. Ikeuchi, "High-resolution hyperspectral imaging via matrix factorization," in *Proc. IEEE Int. Conf. Computer Vision Pattern Recognition*, 2011, pp. 2329–2336.

[72] A. Charles, B. Olshausen, and C. Rozell, "Learning sparse codes for hyperspectral imagery," *IEEE J. Select. Topics Signal Processing*, vol. 5, no. 5, pp. 963–978, 2011.

[73] B. Huang, H. Song, H. Cui, J. Peng, and Z. Xu, "Spatial and spectral image fusion using sparse matrix factorization," *IEEE Trans. Geosci. Remote Sensing*, vol. 52, no. 3, pp. 1693–1704, 2014.

[74] M. Veganzones, M. Simes, G. Licciardi, J. M. B. Dias, and J. Chanussot, "Hyperspectral super-resolution of locally low rank images from complementary multisource data," in *Proc. IEEE Int. Conf. Image Processing*, Paris, France, Oct. 2014, pp. 703–707.

[75] N. Yokoya, T. Yairi, and A. Iwasaki, "Hyperspectral, multispectral, and panchromatic data fusion based on coupled non-negative matrix factorization," in *Proc. IEEE GRSS Workshop Hyperspectral Image Signal Process.: Evolution Remote Sensing*, 2011, pp. 1–4.

[76] D. D. Lee and H. S. Seung, "Learning the parts of objects by nonnegative matrix factorization," *Nature*, vol. 401, pp. 788–791, Oct. 1999.

[77] D. C. Heinz and C.-I. Chang, "Fully constrained least squares linear spectral mixture analysis method for material quantification in hyperspectral imagery," *IEEE Trans. Geosci. Remote Sensing*, vol. 29, no. 3, pp. 529–545, Mar. 2001.

[78] N. Yokoya, N. Mayumi, and A. Iwasaki, "Cross-calibration for data fusion of EO-1/Hyperion and Terra/ASTER," *IEEE J. Select. Topics Appl. Earth Observ. Remote Sensing*, vol. 6, pp. 419–426, Apr. 2013.

[79] L. Wald, T. Ranchin, and M. Mangolini, "Fusion of satellite images of different spatial resolutions: Assessing the quality of resulting image," *IEEE Trans. Geosci. Remote Sensing*, vol. 43, pp. 1391–1402, 2005.

[80] I. Amro, J. Mateos, M. Vega, R. Molina, and A. K. Katsaggelos, "A survey of classical methods and new trends in pansharpening of multispectral images," *EURASIP J. Adv. Signal Processing*, vol. 2011, no. 1, pp. 1–22, 2011.

[81] Q. Du, N. H. Younan, R. L. King, and V. P. Shah, "On the performance evaluation of pan-sharpening techniques," *IEEE Geosci. Remote Sensing Lett.*, vol. 4, pp. 518–522, Oct. 2007.

[82] Z. Wang and A. C. Bovik, "A universal image quality index," *IEEE Signal Processing Lett.*, vol. 9, no. 3, pp. 81–84, Mar. 2002.

[83] L. Alparone, B. Aiazzi, S. Baronti, A. Garzelli, F. Nencini, and M. Selva, "Multispectral and panchromatic data fusion assessment without reference," *Photogramm. Eng. Remote Sens.*, vol. 74, no. 2, pp. 193–200, Feb. 2008.

[84] G. Piella and H. Heijmans, "A new quality metric for image fusion," in *Proc. IEEE Int. Conf. Image Processing*, 2003, vol. 2, pp. 173–176.

[85] L. Wald, *Data Fusion: Definitions and Architectures—Fusion of Images of Different Spatial Resolutions*. Les Presses de l'Ecole des Mines, 2002.

[86] L. Loncan, L. B. Almeida, J. M. Bioucas-Dias, X. Briottet, J. Chanussot, N. Dobigeon, S. Fabre, W. Liao, G. Licciardi, M. Simoes, J.-Y. Tourneret, M. Veganzones, G. Vivone, Q. Wei, and N. Yokoya. (2015). Hyperspectral pansharpening: A review—Complementary results and supporting materials. Tech. Rep., [Online]. Available: http://openremotesensing.net

[87] Q. Wei, N. Dobigeon, and J.-Y. Tourneret, "FUSE: A fast multiband image fusion algorithm," in *Proc. IEEE Int. Workshop Computational Advances Multi-Sensor Adaptive Processing*, Cancun, Mexico, Dec. 2015.

*GRS*